

Comparative study of complex N- and O-bearing molecules in hot molecular cores ★

F. Fontani¹, I. Pascucci², P. Caselli^{3,5}, F. Wyrowski⁴, R. Cesaroni⁵, and C.M. Walmsley⁵

¹ INAF, Istituto di Radioastronomia, CNR, Via Gobetti 101, I-40129 Bologna, Italy

² Steward Observatory, The University of Arizona, Tucson, AZ 85721

³ Harvard-Smithsonian Center for Astrophysics, 60 Garden Street MS42, Cambridge, MA 02138, USA

⁴ Max-Planck-Institut fuer Radioastronomie, Auf dem Huegel 69, 53121 Bonn, Germany

⁵ INAF, Osservatorio Astrofisico di Arcetri, Largo E. Fermi 5, I-50125 Firenze, Italy

Received date; accepted date

ABSTRACT

Aims. We have observed several emission lines of two Nitrogen-bearing (C_2H_5CN and C_2H_3CN) and two Oxygen-bearing (CH_3OCH_3 and $HCOOCH_3$) molecules towards a sample of well-known hot molecular cores (HMCs) in order to check whether the chemical differentiation seen in the Orion-HMC and W3(H_2O) between O- and N-bearing molecules is a general property of HMCs.

Methods. With the IRAM-30m telescope we have observed 12 HMCs in 21 bands, centered at frequencies from 86250 to 258280 MHz.

Results. In six sources, we have detected a number of transitions sufficient to derive their main physical properties. The rotational temperatures obtained from C_2H_5CN , C_2H_3CN and CH_3OCH_3 range from ~ 100 to ~ 150 K in these HMCs. The total column densities of these molecules are of the order of $\sim 10^{15} - 10^{17} \text{ cm}^{-2}$. Single Gaussian fits performed to unblended lines show a marginal difference in the line peak velocities of the C_2H_5CN and CH_3OCH_3 lines, indicating a possible spatial separation between the region traced by the two molecules. On the other hand, neither the linewidths nor the rotational temperatures and column densities confirm such a result. The average molecular abundances of C_2H_5CN , C_2H_3CN and CH_3OCH_3 are in the range $\sim 10^{-9} - 10^{-10}$, comparable to those seen in the Orion hot core. In other HMCs Bisschop et al. 2007 found comparable values for C_2H_5CN but values ~ 2.5 times larger for CH_3OCH_3 . By comparing the abundance ratio of the pair C_2H_5CN/C_2H_3CN with the predictions of theoretical models, we derive that the age of our cores ranges between 3.7 and 5.9×10^4 yrs.

Conclusions. The abundances of C_2H_5CN and C_2H_3CN are strongly correlated, as expected from theory which predicts that C_2H_3CN is formed through gas phase reactions involving C_2H_5CN . A correlation is also found between the abundances of C_2H_5CN and CH_3OCH_3 , and C_2H_3CN and CH_3OCH_3 . In all tracers the fractional abundances increase with the H_2 column density while they are not correlated with the gas temperature. On average, the chemical and physical differentiation between O- and N-bearing molecules

seen in Orion and W3(H₂O) is not revealed by our observations. We believe that this is partly due to the poor angular resolution of our data, which allows us to derive only average values over the sources of the discussed parameters.

Key words. Stars: formation – Radio lines: ISM – ISM: molecules

1. Introduction

The formation process of massive stars ($M \geq 8M_{\odot}$) is still poorly understood. This is mainly due to the observational limitations that hinder the study of early-type stars, i.e. their shorter evolutionary timescales, larger distances and stronger interaction with their environment. Despite this, a growing effort has been devoted to investigate this process, and important results have been obtained both from the observational and the theoretical point of view (see e.g. Garay & Lizano 1999; Tan & McKee 2002; Yorke 2004; Beuther et al. 2007; Cesaroni et al. 2007).

It is well known that when a high-mass star reaches the ZAMS, an ultracompact (UC) HII region, i.e. an ionized region with diameter smaller than a few ~ 0.1 pc, becomes observable at radio wavelengths due to the emission of free-free radiation. This has led to using UC HII regions as “signposts” of massive star formation (e.g. Wood and Churchwell 1989). Various authors have shown that UC HII regions are embedded in molecular clumps of a few thousand solar masses, diameters ~ 1 pc, and average H₂ volume density of $\sim 10^5$ cm⁻³ (Cesaroni et al. 1991; Hofner et al. 2000; Fontani et al. 2002). Observations at higher angular resolution have also identified hot (≥ 100 K), dense ($\geq 10^7$ cm⁻³) and compact (≤ 0.1 pc) molecular condensations in these clumps, called “hot molecular cores” (HMCs) from the name of their prototype, the Orion Hot Core (see Genzel & Stutzki 1989; Walmsley & Schilke 1992). These HMCs are often associated with outflows, water masers, and in some of them an UC HII region has been detected, suggesting that they represent the environment in which high-mass stars were recently born (see e.g. Kurtz et al. 2000; Cesaroni 2005). Their chemical composition is peculiar and very different from that of the surrounding molecular clump, showing higher abundances of saturated species (e.g. H₂O, NH₃, CH₃OH) and complex organic H-rich molecules (see e.g. Caselli 2005).

Since most of the observed H-rich molecules are difficult to form in gas-phase reactions, grain-surface chemistry is often invoked to explain their formation. One possible scenario is the following: during the collapse of a pre-stellar core, molecules freeze out onto dust grains, react with atoms or other molecules on the grain surface and, as the core is heated by the young star, some of them evaporate and return to the gas phase. Based on this scenario, one can distinguish three types of molecules (see Charnley 1995):

Send offprint requests to: F. Fontani, e-mail: ffontani@ira.inaf.it

* Based on observations carried out with the IRAM Pico Veleta telescope. IRAM is supported by INSU/CNRS (France), MPG (Germany) and IGN (Spain).

- those formed in cold gas through ion-molecule reactions, frozen onto dust grains and then released into the gas phase when the core is heated up by the central star. Their abundances should hence reflect those of the initial early cold phase;
- those formed on the grain surfaces through reactions of frozen species, and then evaporated during the HMC phase;
- those formed in hot gas through reactions of evaporated molecules.

Several studies have been made to investigate the chemistry of HMCs (Macdonald et al. 1995; Gibb et al. 2000; Nomura & Millar 2004; Garrod & Herbst 2006). Charnley et al. (1992) showed that initial differences in the chemical composition and gas phase reactions subsequent to evaporation from dust grains can explain the existence of many of the complex O- and N-bearing species. Interestingly, Blake et al. (1987) found that N-bearing species are more abundant than O-bearing ones in the Orion-HC, while the opposite is observed in the Compact Ridge. The chemical model by Caselli et al. (1993) explains such a chemical difference as being due to the different physical properties of the two regions. The model also predicts a relation between the core evolutionary stage and the abundance ratio of molecular species like C_2H_3CN and C_2H_5CN . Therefore, the relative abundance of these species can be used as a 'chemical clock' to estimate the HMC age.

In this work we present the results of the first survey of 4 complex molecules, C_2H_3CN , C_2H_5CN , CH_3OCH_3 and $HCOOCH_3$, towards 12 well-known HMCs, all of them associated with UC HII regions and already observed in several molecular tracers (Hatchell et al. 1998; Hofner et al. 2000; Fontani et al. 2002). In Sect. 2 we describe the observations and we present our sample. The methods used to analyse the data and the immediate results are presented in Sect. 3. In Sect. 4 we discuss our results, and give an estimate of the chemical ages of the HMCs. Conclusions are drawn in Sect. 5.

2. Observations and Data Reduction

2.1. Observations

The observations were carried out with the IRAM 30-m telescope during two observing runs: in July 1996, and August 1997. The observed sources are listed in Table 1: in Cols. 2 and 3 we give the equatorial (J2000) coordinates; LSR source velocities (V_{LSR}) and kinematic distances (d) are given in Cols. 4 and 5, respectively. The numbers listed in Col. 6 will be used in the following to identify the source. We observed simultaneously at 3, 2, and 1.3 mm. The half power beam width (HPBW) of the telescope was $\sim 22''$, $\sim 16''$, and $\sim 12''$, respectively. We obtained spectra of vinyl cyanide (C_2H_3CN), ethyl cyanide (C_2H_5CN), methyl formate ($HCOOCH_3$) and dimethyl ether (CH_3OCH_3). The central frequencies of the observed bands and the sources observed in each band are listed in Table 2.

System temperatures for both observing runs were 300–450 K, 500–900 K, and 700–3000 K for the 3 mm, 2 mm, and 1.3 mm receivers, respectively. The given temperature ranges depend

Table 1. List of the observed sources. The distances are taken from Table 1 of Kurtz et al. (2000) except when differently specified.

Source	R.A.(J2000)	Dec.(J2000)	V_{LSR}	d	code
	(h m s)	($^{\circ}$ $'$ $''$)	(km s^{-1})	(kpc)	
W3(H ₂ O)	02 27 04.7	+61 52 24.5	-45.0	1.95 ^a	1
G5.89-0.39	18 00 30.4	-24 04 00.5	10.0	2.0 ^b	2
G9.62+0.19	18 06 15.0	-20 31 42.2	4.4	5.7	3
G10.47+0.03	18 08 38.2	-19 51 49.7	67.8	5.8	4
G10.62-0.38	18 10 28.7	-19 55 49.7	-3.1	4.8 ^c	5
G19.61-0.23	18 27 38.1	-11 56 38.5	41.6	12.6 ^d	6
G29.96-0.02	18 46 04.0	-02 39 21.5	98.0	7.4	7
G31.41+0.31	18 47 34.4	-01 12 46.0	97.0	7.9	8
G34.26+0.15	18 53 18.5	+01 14 57.7	58.0	3.7 ^e	9
G45.47+0.05	19 14 25.6	+11 09 25.9	62.0	8.3	10
W51D	19 23 39.9	+14 31 08.1	60.0	8.0	11
IRAS20126+4104	20 14 26.0	+41 13 32.5	-3.5	1.7	12

R.A.(J2000)= right ascension

Dec.(J2000)= declination

V_{LSR} = Local standard of rest velocity

^a Xu et al. (2006)

^b Acord et al. (1998)

^c Fish et al. (2003)

^d Kolpak et al. (2003)

^e Kuchar & Bania (1994)

on weather conditions and source elevation. The receivers alignment was checked through continuum cross scans on planets and found to be accurate to within 2'' for the 3 mm, 2 mm, and the first 1.3 mm receiver. A misalignment of up to 5'' was observed for the second 1.3 mm receiver, which however is negligible with respect to the beam size. Our spectrometers were an autocorrelator with bandwidth ~ 523 MHz and 0.32 MHz resolution, and two filter-banks with 512 MHz bandwidth and 1 MHz resolution. The wobbling secondary mirror was used with a beam throw of 240'' and a frequency of 0.5 Hz resulting in linear baselines of the spectra. The focus was checked at the beginning of each night on Jupiter or Saturn. Since the two 1.3 mm receivers had somewhat different foci, we selected in these cases a focus position giving a compromise between the different receivers more weighted to the 1.3 mm G1 receiver that had the same focus as the 3 and 2 mm receivers. The resulting gain loss is smaller than 10%. Pointing was checked hourly by cross scans on planets. The observations were made in wobbler switching mode, with

the wobbling secondary reflector switching in azimuth at a rate of 0.5 Hz between the source position and a reference position offset by 4 arcmin.

The data were reduced and analysed using the software package CLASS. An advanced version of the package, XCLASS, was used to fit the transitions with blending problems (see e.g. Comito et al. 2005 for details on the XCLASS fitting procedure).

2.2. Line Identification

Line identification was done using several catalogues of line frequencies: the Lovas¹ and JPL² catalogues, as well as the compilations of Anderson et al. (1987, 1988a, 1988b, 1990a, 1990b, 1992), Bettens et al. (1999), Groner et al. (1998), Herbst (1999), Klisch et al. (1996), Pan et al. (1998), Pearson et al. (1991, 1994, 1997), Plummer et al. (1986, 1987), Wyrowski et al. (1999), Yamada et al. (1986). Predicted vibrational transitions of C₂H₅CN were taken from Pearson (2002). We have considered as identified those lines in the spectra within ~ 1 MHz from the expected line position in the catalogues. We have considered as detected the lines above the 3σ level in the spectra.

In Fig. 1 we show a sample spectrum at 3 mm for the source G34.26+0.15, with identified and unidentified lines.

3. Results

In this Section we report on and analyse the results for the 6 sources of our sample which show a number of transitions sufficient to derive the physical parameters of our interest (column density, temperature, abundance). They are listed in Col. 1 of Table 3. All spectra observed towards these sources are shown in Figures A-1 – A-11 of Appendix A. Hereafter, we will use the source name G10.47 for G10.47+0.03, G10.62 for G10.62–0.38, G19.61 for G19.61–0.23, G29.96 for G29.96–0.02, G31.41 for G31.41+0.31 and G34.26 for G34.26+0.15.

We will concentrate on the study of C₂H₃CN, C₂H₅CN, and CH₃OCH₃. We discuss separately the results of the study of HCOOCH₃ in Sect. 3.3, because most of the transitions of this molecule appear in multiplets with nearly the same upper energies, and they are blended with lines of other molecular species much more than the lines of C₂H₅CN, C₂H₃CN and CH₃OCH₃.

3.1. Masses and H₂ Column Densities of the cores

To derive the abundances of the observed molecules relative to H₂ we need first to estimate the total gas mass, M_{gas} . We have computed M_{gas} and the corresponding H₂ total column density, $N(\text{H}_2)$, assuming the clumps to be Gaussian and in virial equilibrium. Under the further hypoth-

¹ <http://physics.nist.gov/PhysRefData/Micro/Html/contents.html>

² <http://spec.jpl.nasa.gov>

Table 2. Observed frequency bands

Observing run	Band name	ν_c^a (MHz)	observed sources ^b
July 1996	BAND3–HCN	86250	1,4,8
	BAND3–HNCO	87800	1,4,7,8
	BAND3–109	109410	4,8
	BAND3–110	110095	1,4,5,7-9
	BAND2–NH3	140300	4,8
	BAND2–154	154230	1,4,7,8
	BAND2–155	154850	1,4,5,7-9
	BAND1–215	215250	1,4,5,7-9
	BAND1–218	218970	1,4,8
	BAND1–HNCO	219580	1,4,7,8
August 1997	BAND1–228	228100	4,8
	BAND1–HCN	258280	1,4,8
	BAND3MM-1	98600	4-9,11,12
	BAND3MM-2	104360	6-9,11
	BAND3MM-3	111600	1-12
	BAND2MM-1	147370	1-12
	BAND2MM-2	161463	4-9,11,12
	BAND2MM-3	173150	6-9,11
	BAND1MM-1	209580	6-9,11
	BAND1MM-2	224237	1-12
	BAND1MM-3	237460	4-9,11,12

^a band central frequency^b source identification numbers as in Table 1

esis that the lines are not broadened by high optical depth, one can demonstrate that M_{gas} and N_{H_2} are given by:

$$M_{\text{gas}}(M_{\odot}) = 125 \Delta v^2 (\text{km s}^{-1}) D(\text{pc}) , \quad (1)$$

$$N_{\text{H}_2} = \frac{4 \ln 2}{\pi D^2 m_{\text{H}_2}} M_{\text{gas}} , \quad (2)$$

where Δv is the observed full line width at half maximum, $D = d\theta_s$ is the HMC linear diameter (θ_s is the source angular diameter) and m_{H_2} is the mass of the H_2 molecule.

The results are summarised in Table 3: HMC angular and linear diameters (obtained from the literature) are listed in Cols. 2 and 3, respectively; line widths, core masses and H_2 total column densities are given in Cols. 4, 5 and 6, respectively. The source linear diameters have been computed from the distances in Table 1. The line widths are the average values of isolated

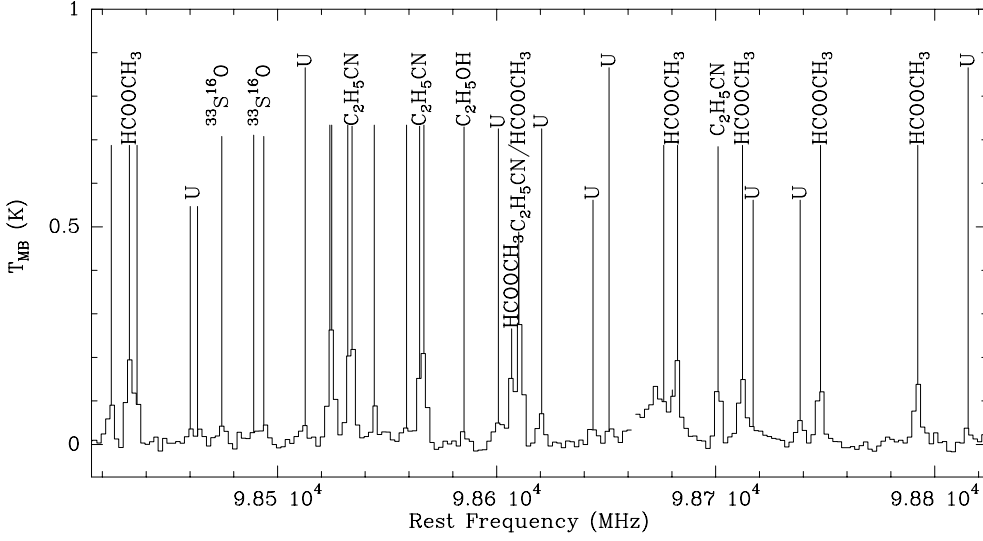


Fig. 1. Spectrum of G34.26+0.15 in BAND3MM-1. The identified and unidentified (U) lines are marked.

Table 3. Source angular (θ_s) and linear (D) diameters, linewidths at half of the maximum of the C_2H_5CN transitions ($\Delta\nu$), core masses (M_{gas}) and H_2 total column densities ($N(H_2)$). The diameters are derived from mm interferometric data, except when otherwise specified. Masses and column densities are computed assuming sources in virial equilibrium and with Gaussian distribution of the gas.

Source	Diameter		$\Delta\nu$ (km s ⁻¹)	M_{gas} (M _⊙)	$N(H_2)$ (cm ⁻²)
	θ_s	D			
	($''$)	(pc)			
G10.47+0.03	1.3 ^a	0.036	7.89	286	1.2×10^{25}
G10.62−0.38	1.7 ^b	0.039	5.18	133	4.8×10^{24}
G19.61−0.23	1.9 ^c	0.112	9.34	1239	5.4×10^{24}
G29.96−0.02	1.4 ^d	0.050	6.01	228	5.1×10^{24}
G31.41+0.31	1.1 ^e	0.042	8.52	385	1.2×10^{25}
G34.26+0.15	3.6 ^f	0.066	6.55	358	4.5×10^{24}

^a Olmi et al. (1996)

^b Keto et al. (1988, from NH_3 interferometric observations)

^c Kurtz et al. (2000)

^d Cesaroni et al. (1998, from NH_3 interferometric observations)

^e Beltrán et al. (2005)

^f Akeson & Carlstrom (1996, from CH_3CN interferometric observations)

transitions of C_2H_5CN . We decided to use this molecule because it is the species for which we have the largest number of unblended lines in each source.

The angular diameters of the HMCs have been taken from previous interferometric observations and require a detailed discussion. Most of the cores of our sample have been already

observed at high angular resolution in several molecular tracers, such as e.g. NH_3 , CH_3CN and CH_3OH . These observations have shown that different molecular species can probe distinct regions of the core. Beuther et al. (2005) have observed at high angular resolution the Orion-HC in several molecular tracers, and reported significant spatial separation among the regions traced by O-, N- and S-bearing species (see also Fig. 2 of Wright et al. 1996). Notwithstanding this, at present high angular resolution observations of complex molecules in the HMCs of our sample are poor: Beltrán et al. (2005) have detected one line of $\text{C}_2\text{H}_5\text{CN}$ and HCOOCH_3 in G31.41, and found that their integrated emission maps are fairly well overlapping with that of the 1.4 mm continuum, even though the two species do not peak exactly at the same position (see their Fig. 26). Similarly, Mookerjee et al. (2007) have detected few lines of $\text{C}_2\text{H}_5\text{CN}$, HCOOCH_3 and CH_3OCH_3 in G34.26, showing a separation between the emission peaks of O- and N-bearing species of $\sim 0''.8$, but a substantial overlap between their emission maps and that of the 2.8 mm continuum. Additionally, Remijan et al. (2004) have found that in G19.61, HCOOCH_3 and $\text{C}_2\text{H}_5\text{CN}$ approximately peak at the same position. Given these results, as zero-order assumption we will suppose that the emission of all the observed molecules arises from the region seen in the mm continuum.

The angular diameters listed in Table 3 are hence derived from mm continuum interferometric maps with the exception of three sources: G10.62, G29.96 and G34.26. We decided to use the diameter inferred from CH_3CN for G34.26 and from NH_3 for G29.96, respectively, instead of that from the mm continuum, because the mm continuum position does not agree with that of the molecular emission (see Akeson & Carlstrom 1996 and Carral & Welch 1992 for G34.26; Olmi et al. 2003 for G29.96). Also, in G34.26 60% of the mm flux is due to the free-free continuum emission of an associated HII region (Akeson & Carlstrom 1996). For G10.62, angular diameters from mm continuum interferometric data are not available. Therefore, we have assumed the diameter from NH_3 inversion transitions measurements.

The total H_2 column density has been derived in our sources also from C^{17}O by Hofner et al. (2000) and from $\text{CH}_3\text{C}_2\text{H}$ by Fontani et al. (2002). In both works the authors used Eq. (1), adopting the diameters and the virial masses they derive from the molecular lines that they observed. These estimates are ~ 2 orders of magnitude lower than those obtained from $\text{C}_2\text{H}_5\text{CN}$, consistently with the fact that the C^{17}O and $\text{CH}_3\text{C}_2\text{H}$ transitions trace the parsec-scale molecular clump in which the HMC is embedded.

3.2. Rotational temperatures, total column densities and fractional abundances

3.2.1. Derivation of the parameters

We derive rotational temperatures and total column densities applying the population diagram method described by Goldsmith & Langer (1999, hereafter GL99). The main assumptions in this method are: (i) optically thin lines; (ii) local thermodynamic equilibrium (LTE) conditions.

Under assumption (i), one can compute the column density N_u of the upper level, u , of each transition from its integrated intensity according to the relation:

$$\frac{N_u}{g_u} = \frac{3k}{8\pi^3} \frac{W}{\nu \mu^2 S} \quad (3)$$

where g_u is the statistic weight of the upper level, k the Boltzmann constant, W the integrated line intensity (in K km s⁻¹), ν the line rest frequency, μ the molecule's dipole moment and S the line strength. Then, under assumption (ii), we can use Eq. (21) of GL99 to derive rotational temperatures and total column densities of the molecules from least square fits to the data. The validity of assumptions (i) and (ii) will be discussed in detail in Sect. 3.2.4. The parameters derived from the XCLASS fitting procedure for the lines identified and used in the rotation diagrams are given for each source in Tables .1 - .11 of Appendix B. The rotation diagrams for all sources are shown in Figs. .1 - .6 of Appendix C.

The nuclear spin degeneracy and the partition functions used in Eq. (21) of GL99 have been taken from Blake et al. (1987) and Turner et al. (1991) for C₂H₅CN, C₂H₃CN, and HCOOCH₃, and from Groner et al. (1998) for CH₃OCH₃. Partition functions are calculated analytically in the approximation of high temperatures (i.e. $hA \ll kT$ for asymmetric top species, where A is the Einstein coefficient). For the vibrational transitions, we computed the partition function following the approximation of Nummelin & Bergman (1999). In the rotation diagrams, the column density of each level observed at 2 mm and 1.3 mm has been normalized to the telescope beam at 3 mm ($\sim 23''$) assuming a source diameter negligible with respect to the beam size, thus obtaining *beam-averaged* total column densities. Then, *source-averaged* total column densities have been inferred by multiplying the beam-averaged values by $(23/\theta_s)^2$.

The molecule's fractional abundance, X , is given by the source-averaged total column density divided by the H₂ total column density listed in Col. 5 of Table 3: $X = N(\text{molecule})/N(\text{H}_2)$.

3.2.2. Temperatures and column densities

Rotational temperatures (T), beam- and source-averaged total column densities (N_b and N_s) are given in Cols. 3, 4 and 5 of Tab. 4, respectively.

The rotational temperatures typically range from ~ 100 to ~ 150 K in all tracers. In each source, the estimates obtained from C₂H₅CN, C₂H₃CN and CH₃OCH₃ are in good agreement among them, with the exception of G34.26 and G10.62. For G34.26, the estimate from C₂H₃CN is a factor of 2 lower than those derived from CH₃OCH₃ and C₂H₅CN, but this is likely due to the fact that in the rotation diagram there are no points above ~ 200 K. In G10.62, the temperature from CH₃OCH₃ is much lower (~ 16 K) than the other two estimates, but it has been obtained from only few line detections and is thus less accurate.

The temperatures derived from C₂H₅CN and CH₃OCH₃ are in agreement both with those obtained by Bisschop et al. (2007) in other HMCs, and with those derived from other HMC tracers by Kurtz et al. (2000, see their Table 1), further attesting they are tracing the hot gas of the cores. The column densities of C₂H₅CN are in good agreement with the values of Bisschop et

Table 4. Rotational temperatures (T), beam and source averaged total column densities (N_b and N_s) and abundances (X) with respect to H_2 of C_2H_5CN , C_2H_3CN and CH_3OCH_3 .

Molecule	Source	T (K)	N_b (cm^{-2})	N_s (cm^{-2})	X
C_2H_5CN	G10.47	103 \pm 12	3.6 \pm 0.9 $\times 10^{14}$	1.1 \pm 0.3 $\times 10^{17}$	9.6 $\times 10^{-9}$
	G10.62	89 \pm 13	2.5 \pm 0.9 $\times 10^{13}$	4.6 \pm 1.6 $\times 10^{15}$	9.5 $\times 10^{-10}$
	G19.61	116 \pm 12	1.5 \pm 0.2 $\times 10^{14}$	2.2 \pm 0.3 $\times 10^{16}$	4.1 $\times 10^{-9}$
	G29.96	121 \pm 17	5.4 \pm 1.3 $\times 10^{13}$	1.5 \pm 0.3 $\times 10^{16}$	3.0 $\times 10^{-9}$
	G31.41	118 \pm 13	2.3 \pm 0.5 $\times 10^{14}$	1.0 \pm 0.2 $\times 10^{17}$	8.3 $\times 10^{-9}$
	G34.26	130 \pm 13	1.9 \pm 0.3 $\times 10^{14}$	8.4 \pm 1.3 $\times 10^{15}$	1.9 $\times 10^{-9}$
C_2H_3CN	G10.47	176 \pm 35	2.0 \pm 0.6 $\times 10^{14}$	6.1 \pm 1.7 $\times 10^{16}$	5.1 $\times 10^{-9}$
	G10.62	–	$\leq 1.7 \times 10^{13}$	$\leq 3.2 \times 10^{15}$	$\leq 6.8 \times 10^{-10}$
	G19.61	123 \pm 24	6.5 \pm 2.1 $\times 10^{13}$	9.7 \pm 3.2 $\times 10^{15}$	1.8 $\times 10^{-9}$
	G29.96	fixed	2.7 $\times 10^{13}$	7.3 $\times 10^{15}$	1.4 $\times 10^{-9}$
	G31.41	111 \pm 12	8.4 \pm 1.8 $\times 10^{13}$	3.7 \pm 1.0 $\times 10^{16}$	3.1 $\times 10^{-9}$
	G34.26	67 \pm 15	5.6 \pm 2.5 $\times 10^{13}$	2.4 \pm 1.0 $\times 10^{15}$	5.3 $\times 10^{-10}$
CH_3OCH_3	G10.47	156 \pm 37	1.2 \pm 0.3 $\times 10^{14}$	3.9 \pm 1.0 $\times 10^{16}$	3.3 $\times 10^{-9}$
	G10.62	16 \pm 1	1.4 \pm 0.2 $\times 10^{13}$	2.6 \pm 0.4 $\times 10^{15}$	5.4 $\times 10^{-10}$
	G19.61	158 \pm 17	1.3 \pm 0.1 $\times 10^{13}$	2.0 \pm 0.2 $\times 10^{15}$	3.7 $\times 10^{-10}$
	G29.96	141 \pm 26	2.3 \pm 0.4 $\times 10^{13}$	6.2 \pm 1.0 $\times 10^{15}$	1.2 $\times 10^{-9}$
	G31.41	127 \pm 25	7.9 \pm 1.9 $\times 10^{13}$	3.5 \pm 1.0 $\times 10^{16}$	2.9 $\times 10^{-9}$
	G34.26	116 \pm 25	7.6 \pm 2.3 $\times 10^{13}$	3.3 \pm 1.0 $\times 10^{15}$	7.3 $\times 10^{-10}$

al. (2007) in similar objects, while for CH_3OCH_3 we find column densities one order of magnitude smaller. In computing source-averaged column densities Bisschop et al. (2007) assume a source diameter corresponding to that of the region where the temperature is higher than ~ 100 K, that is comparable to those of our objects ($\sim 1''$). Since masses and luminosities of the cores are comparable as well, the observed difference might reflect a different CH_3OCH_3 chemistry in the HMCs of our sample and those of Bisschop et al. (2007).

Only three transitions of C_2H_3CN have been identified towards G29.96. In this case the column densities have been estimated fixing the rotation temperature to that found from C_2H_5CN . The assumption of equal rotational temperature for C_2H_3CN and C_2H_5CN is justified both by observations (Schilke et al. 1997), which have shown that these molecules trace a very similar region, and by chemical models (Charnley et al. 1992; Caselli et al. 1993), which predict that C_2H_3CN forms in gas phase reactions involving C_2H_5CN .

3.2.3. Molecular fractional abundances

Molecular fractional abundances are listed in Col. 6 of Table 4. The average abundances of $\text{C}_2\text{H}_5\text{CN}$, $\text{C}_2\text{H}_3\text{CN}$ and CH_3OCH_3 are $\sim 4.6 \times 10^{-9}$, 2.4×10^{-9} and $\sim 1.5 \times 10^{-9}$, respectively. These values are comparable to those found in the Orion Hot Core (Sutton et al. 1995) and in Sgr B2 (Nummelin et al. 2000). $\text{C}_2\text{H}_5\text{CN}$ abundances are also comparable to the values obtained by Bisschop et al. (2007) in a similar sample of HMCs, while for CH_3OCH_3 we find a discrepancy of ~ 2 orders of magnitude with respect to the estimates of Bisschop et al. (2007). Again, we have to consider that in deriving their H_2 column densities Bisschop et al. (2007) use a model with a power-law density profile in the HMC of the type $n \propto r^{-1.5}$. Since we derive H_2 total column densities directly from observational measurements, the observed difference might be due to some assumptions in the model used by Bisschop et al. (2007) which cannot be applied to our sources.

3.2.4. LTE conditions and optical depth of the lines

Our results have been derived assuming LTE conditions. The critical densities of the observed transitions are of the order of $10^6 - 10^7 \text{ cm}^{-3}$ (see Genzel 1991 for the collisional coefficients), and always $\leq 10^8 \text{ cm}^{-3}$. Assuming spherical and homogeneous cores, from the linear diameters and gas column densities listed in Cols. 3 and 6 of Tab. 3, respectively, we find that all of our HMCs have H_2 volume densities larger than 10^7 cm^{-3} . This makes us confident that the LTE approximation is correct.

The other fundamental assumption of the rotation diagram method is that of optically thin lines. If the lines are optically thick, the expression for the column density of the upper levels given in Eq. (2) has to be multiplied by the factor $\tau/(1 - \exp(-\tau))$ (see e.g. Eq. 16 of GL99), where τ is the line opacity. Such a correction modifies the results of the rotation diagrams: large optical depths are expected to affect mostly the low-excitation transitions, thus causing a flattening of the plots at lower energies. In this case, the temperatures estimated assuming optically thin lines have to be taken as upper limits.

Line opacities can be derived from the line intensity ratio of two isotopologues of the same species. With the help of the JPL catalogue, we checked whether rotational transitions of isotopologues of the molecules of interest fall in the observed frequency bands. We have not found lines of the $\text{C}_2\text{H}_3\text{CN}$ isotopologues: this is likely due to the fact that not all of the line frequencies have been determined yet in the laboratory. On the other hand, the observed bandwidths cover 7 lines of $\text{C}_2\text{H}_5\text{CN}$ isotopologues (5 $\text{CH}_3\text{C}^{13}\text{H}_2\text{CN}$ lines and 2 $\text{CH}_3\text{CH}_2\text{C}^{13}\text{N}$ lines), but they are all undetected. Therefore, we can derive only upper limits on their optical depth: assuming a $^{12}\text{C}/^{13}\text{C}$ ratio of 10, the minimum upper limit turns out to be $\tau = 1.7$ which is not sufficient to conclude that the $\text{C}_2\text{H}_5\text{CN}$ lines are optically thin. Nevertheless, the good agreement between the data and the linear fits indicates that the assumption of optically thin lines is reasonable in our sources.

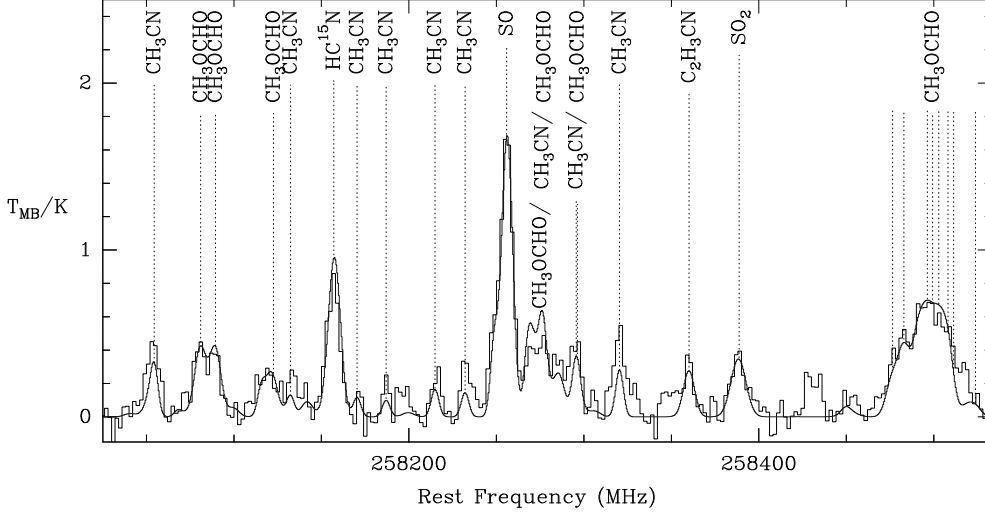


Fig. 2. Sample spectrum of HCOOCH_3 in BAND1-HCN towards the source G10.47. We used the XCLASS software to solve the blending problem in this frequency band.

3.3. HCOOCH_3

As pointed out in Sec. 3, many HCOOCH_3 transitions are blended with other lines. Therefore, we used the software XCLASS to solve this problem (see Sect. 2). The spectra in BAND1-HCN offer the only opportunity in our data sets to fit simultaneously many HCOOCH_3 lines with energy of the upper level from about 150 to 300 K. In Fig. 2 we show an example spectrum at 258500 MHz with highly blended lines fitted by XCLASS. The rotation diagrams of only two sources, G10.47 and G31.41, give reliable fit results. Although the temperature is not well determined by the fit, the total column density is quite accurate since it accounts mainly for the total intensity of the blended feature. We derive source averaged total column densities of $3.7 \times 10^{17} \text{ cm}^{-2}$ for G10.47 and $5.3 \times 10^{17} \text{ cm}^{-2}$ for G31.41. The HCOOCH_3 fractional abundances are therefore $\sim 3.1 \times 10^{-8}$ and $\sim 4.4 \times 10^{-8}$ for G10.47 and G31.41, respectively. Both column densities and abundances are consistent with the values found by Bisschop et al. (2007) in similar HMCs.

3.4. *Vibrationally excited $\text{C}_2\text{H}_3\text{CN}$ in G10.47*

Several lines of vibrationally excited $\text{C}_2\text{H}_3\text{CN}$ have been identified at 218 GHz (see Fig. 3) towards the source G10.47. The main line parameters are given in Table 5. These lines have been identified for the first time by Nummelin et al. (1998) in the Sagittarius B2 molecular cloud. The frequencies for the in-plane CCN bend ν_{11} at 342 K and the CCN out-of-plane bend ν_{15} at 486 K are taken from the JPL catalogue (Poynter & Pickett 1985, Pickett et al. 1996).

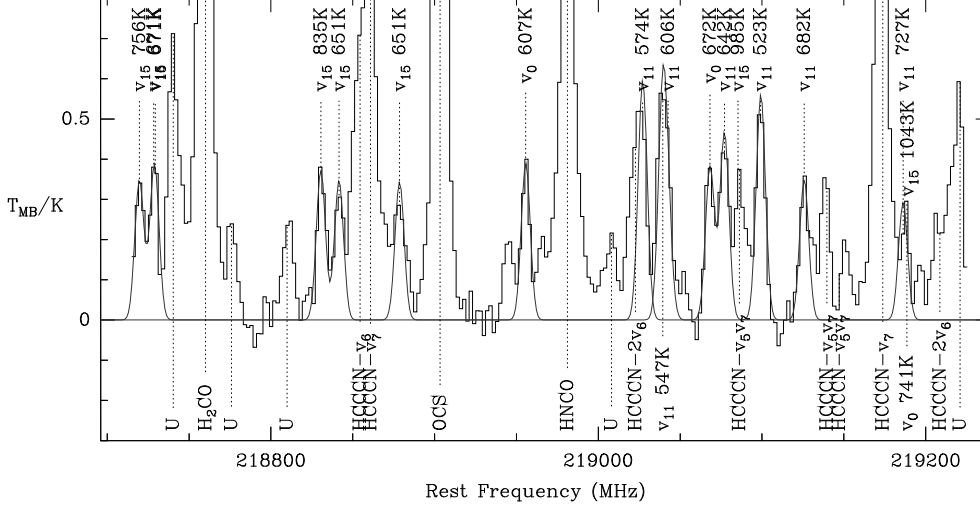


Fig. 3. Vibrationally excited vinyl cyanide in G10.47 at 218 GHz. The lines are marked with their vibrational mode and upper energies are given.

Table 5. Rest frequency (ν), energy of the upper level (E_u) and integrated intensity ($\int T_{MB} d\nu$) of 9 unblended vibrational lines of C_2H_3CN detected towards G10.47.

ν (MHz)	E_u (K)	$\int T_{MB} d\nu$ (K km s ⁻¹)
218719.6	756	3.23
218728.9	671	4.15
218830.5	835	3.57
218841.6	651	3.31
218878.6	651	3.28
219027.1	574	5.68
219077.1	642	4.71
219099.1	523	5.81
219125.8	682	3.46

We also have found two “weak” C_2H_3CN transitions (i.e. transitions with low μ^2S , at $E_u < 100$ K, see Fig. .1). Both vibrational and “weak” lines are unlikely to be optically thick. Therefore, we combine them to derive both temperature and column density. We obtain a rotational temperature of 135 ± 13 K and a source averaged total column density of $1.3 \pm 0.6 \times 10^{18}$ cm⁻². The temperature is equal, within the error bar, to that given in Tab. 4 but the density is about a factor of 20 higher. Note that it is also a factor of 10 higher than C_2H_5CN column den-

Table 6. Rest frequency (ν), energy of the upper level (E_u) and integrated intensity ($\int T_{\text{MB}} d\nu$) of 12 unblended vibrational lines of $\text{C}_2\text{H}_3\text{CN}$ detected towards G10.47 and G31.41.

Source	ν (MHz)	E_u (K)	$\int T_{\text{MB}} d\nu$ (K km s ⁻¹)
G10.47	98464	410	2.0466
	98539	409	0.85978
	98619	361	5.3485
	98672	377	1.9452
	161338	422	3.4767
	224380	342	2.9466
	224396	616	2.1549
	224409	542	2.8934
	224480	522	2.7522
G31.41	98464	410	0.64
	98619	361	1.83
	98672	377	1.27
	98737	342	1.90
	161338	422	2.35
	224378	577	4.28
	224408	542	3.63
	224479	522	2.06

sity (see Tab. 4). The presence of both ”weak” rotational and vibrational lines suggest that some ”strong” rotational transitions can suffer from high optical depth. Therefore, correcting the data following the method described in Sect. 3.2.4, we obtain a best fit for the following parameters: $N_s = (2.3 \pm 0.4) \times 10^{18} \text{ cm}^{-2}$, $T = 133 \pm 3 \text{ K}$, and $\theta \sim 1.6''$.

3.5. *Vibrationally excited $\text{C}_2\text{H}_5\text{CN}$ in G10.47 and G31.41*

Using the compilation of Pearson (2002), we have searched for vibrationally excited $\text{C}_2\text{H}_5\text{CN}$ transitions. We have identified 9 lines in G10.47 and 8 in G31.41. In Fig. 4 and Fig. 5, we show the 3 bands in which vibrationally excited lines of $\text{C}_2\text{H}_5\text{CN}$ have been identified. The main parameters of the identified lines are listed in Table 6. Vibrationally excited $\text{C}_2\text{H}_5\text{CN}$ was firstly identified by Mehrgier et al. (2004) in Sgr B2.

4. Discussion

4.1. *Comparison between N-bearing and O-bearing molecules*

A different spatial distribution between N-bearing and O-bearing molecules has been observed in some HMCs (see Blake et al. 1987, Wright et al. 1992, 1996, and Beuther et al. 2005 for Orion;

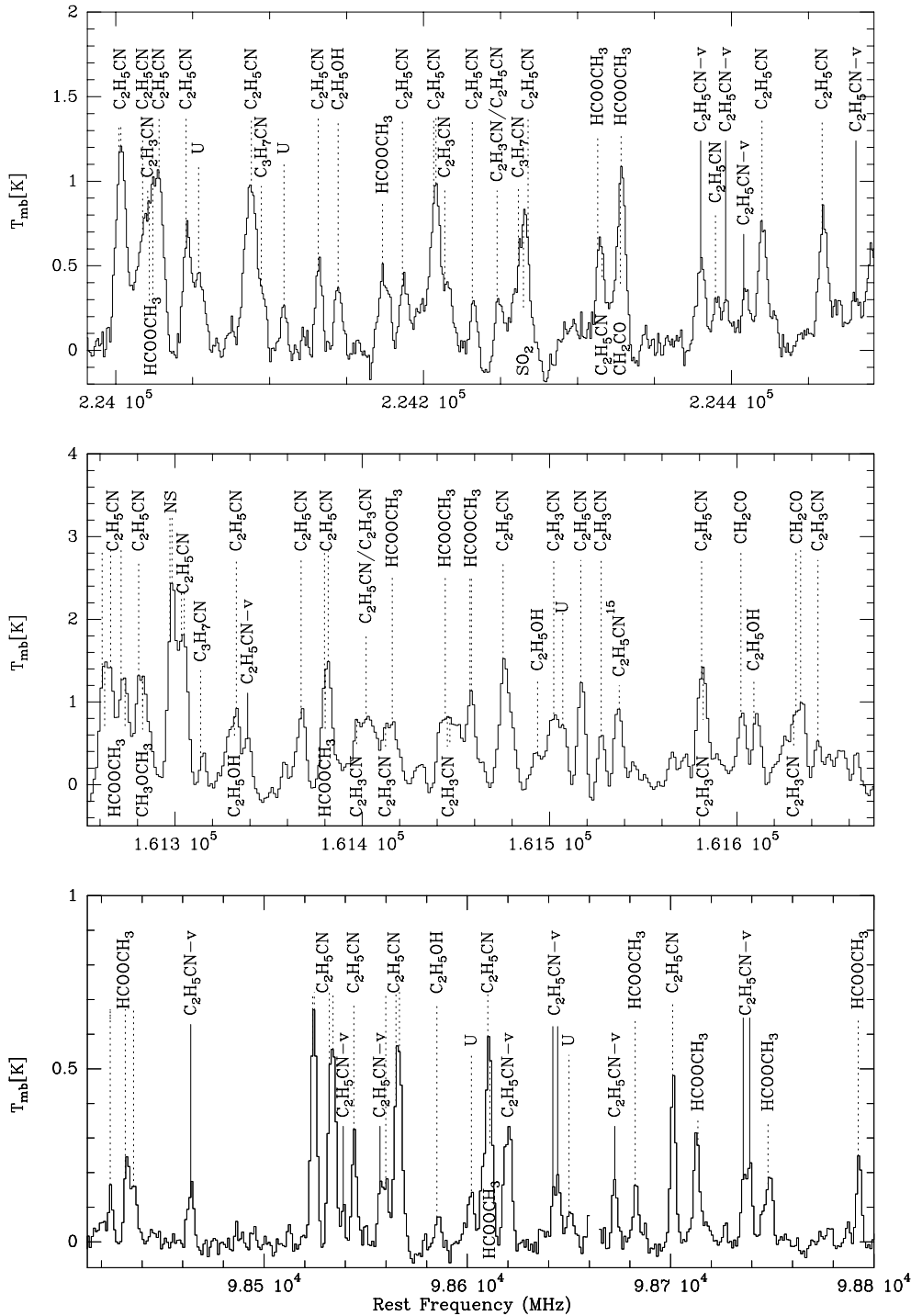


Fig. 4. Bands in which vibrationally excited $\text{C}_2\text{H}_5\text{CN}$ transitions have been identified (solid line) towards the source G10.47.

Wyrowski et al. 1999 for $\text{W3(H}_2\text{O)}$). Caselli et al. (1993) interpreted the difference seen in Orion as being due to the fact that N-bearing and O-bearing species trace regions of the HMCs with different physical properties. Charnley et al. (1992) simply use different grain mantle compositions for the Orion-HC and Compact Ridge to reproduce the observed differentiation.

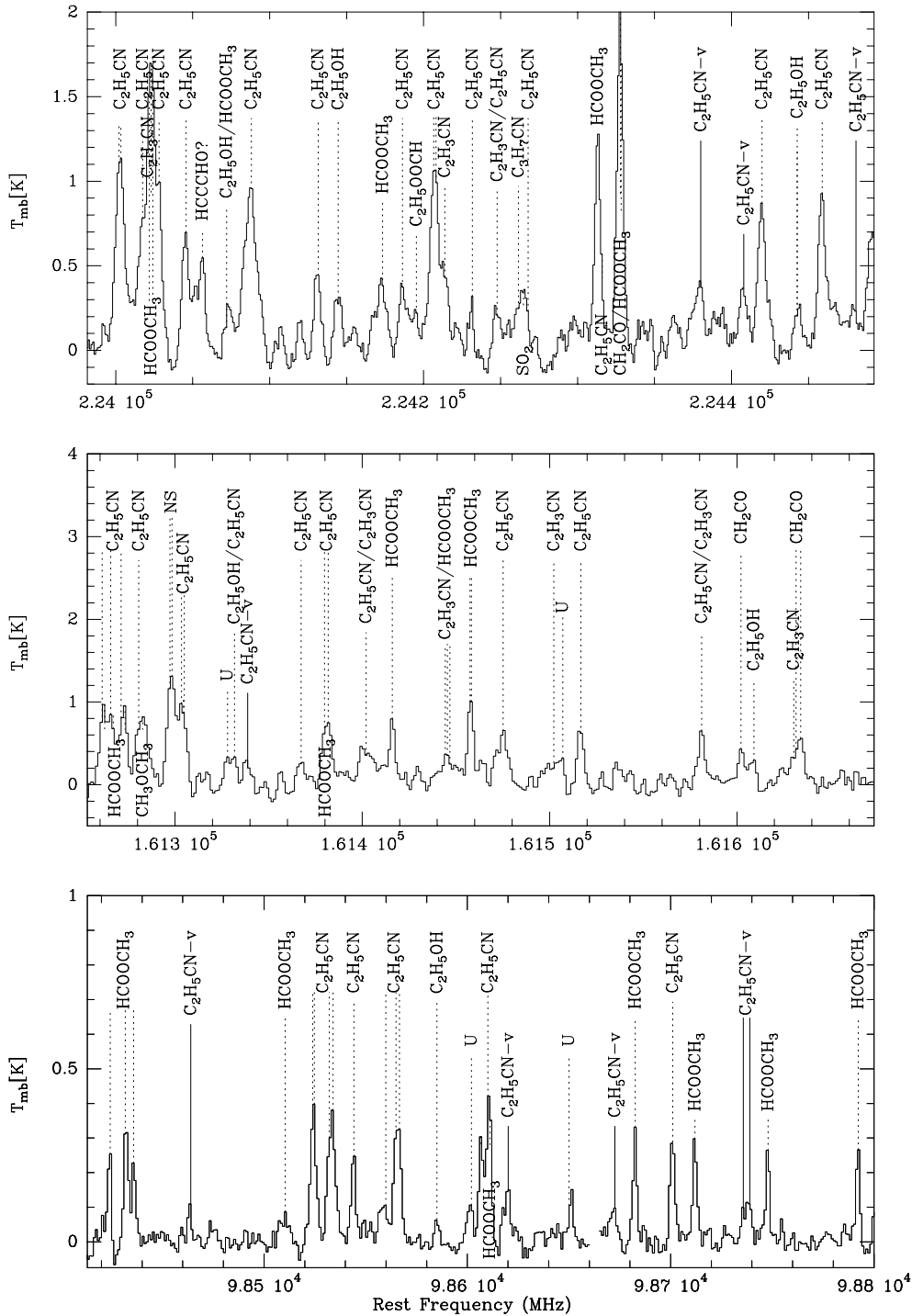


Fig. 5. Bands in which vibrationally excited C₂H₅CN transitions have been identified (solid line) towards the source G31.41.

In order to see if such a differentiation is observable in the HMCs of our sample, we compare in each source the main physical properties (velocity, column density, temperature and abundance) obtained from N- and O-bearing species.

4.1.1. Line velocities and widths at half maximum

Peak velocities, V_{LSR} , and line widths at half maximum, ΔV , of the unblended lines detected in each source are listed in Cols. 3 and 4, respectively, of Table 7. Both V_{LSR} and ΔV have been obtained from single Gaussian fits to the lines. In Cols. 2 and 3 of Table 8 we report the average values of V_{LSR} for the unblended lines of $\text{C}_2\text{H}_5\text{CN}$, V_{N} , and CH_3OCH_3 , V_{O} , respectively, and their difference ($V_{\text{N}} - V_{\text{O}}$) is given in Col. 4. In Cols. 5, 6 and 7 of the same Table we also list the average value of the linewidths for $\text{C}_2\text{H}_5\text{CN}$, ΔV_{N} , and CH_3OCH_3 , ΔV_{O} , and their ratio ($\Delta V_{\text{N}}/\Delta V_{\text{O}}$), respectively.

The velocity differences $V_{\text{N}} - V_{\text{O}}$ and line width ratios $\Delta V_{\text{N}}/\Delta V_{\text{O}}$ found in each source are then plotted in Fig. 6. $V_{\text{N}} - V_{\text{O}}$ shows that on average the $\text{C}_2\text{H}_5\text{CN}$ lines have different velocities from the CH_3OCH_3 lines, in agreement with the idea that they are tracing different regions. The largest difference is for G10.62, for which however we stress that V_{N} has been derived from 3 lines only, and one of these (the line at 224045 MHz) has a very uncertain velocity. On the other hand, no systematic differences are present in the line widths, except for G19.61 for which the $\text{C}_2\text{H}_5\text{CN}$ lines are more than ~ 1.5 times larger than the CH_3OCH_3 lines. We point out that the values plotted in Fig. 6 are *average* values between lines observed at different wavelengths, and this can influence a lot the discussion of these quantities. In fact, the higher excitation lines, which trace the denser and hotter portion of the HMC, are also expected to have highest linewidths. Therefore, the number of unblended lines detected in each band, which are different for each source, may influence the average values both of velocities and linewidths. Also, each rotational transition of CH_3OCH_3 is split into four components coming from torsional motions of the molecule. The separation of these components in velocity is much smaller than the spectral resolution of our data, so that they are not resolved. Even though the software can derive the intrinsic ΔV and V_{LSR} from the theoretical separation of the different components, we believe that ΔV and V_{LSR} from these lines are less accurate than those derived from $\text{C}_2\text{H}_5\text{CN}$. For these reasons, we stress that the quantities plotted in Fig. 6 have to be interpreted carefully.

4.1.2. Abundance correlations

The abundances relative to H_2 of $\text{C}_2\text{H}_5\text{CN}$, $\text{C}_2\text{H}_3\text{CN}$ and CH_3OCH_3 are compared in Figure 7. For each pair of tracers, we have performed a least square fit to the data to check a possible correlation between the different abundances. The left panel of Figure 7 shows that the abundances of the two N-bearing molecules, $\text{C}_2\text{H}_5\text{CN}$ and $\text{C}_2\text{H}_3\text{CN}$, are strongly correlated (correlation coefficient $r \sim 0.96$). This result agrees with the theoretical prediction that $\text{C}_2\text{H}_3\text{CN}$ is produced through gas-phase reactions involving $\text{C}_2\text{H}_5\text{CN}$ (Caselli et al. 1993). On the other hand, central and right panels of Figure 7 show that there is correlation also between the abundances of $\text{C}_2\text{H}_5\text{CN}$ and $\text{C}_2\text{H}_3\text{CN}$, and that of CH_3OCH_3 (correlation coefficients ~ 0.90 and ~ 0.86 , respectively). CH_3OCH_3 is thought to form both through reactions on grain surfaces ($\text{CH}_3 + \text{CH}_3\text{O} \rightarrow \text{CH}_3\text{OCH}_3$, Allen & Robinson 1977), and in the gas phase through reactions between

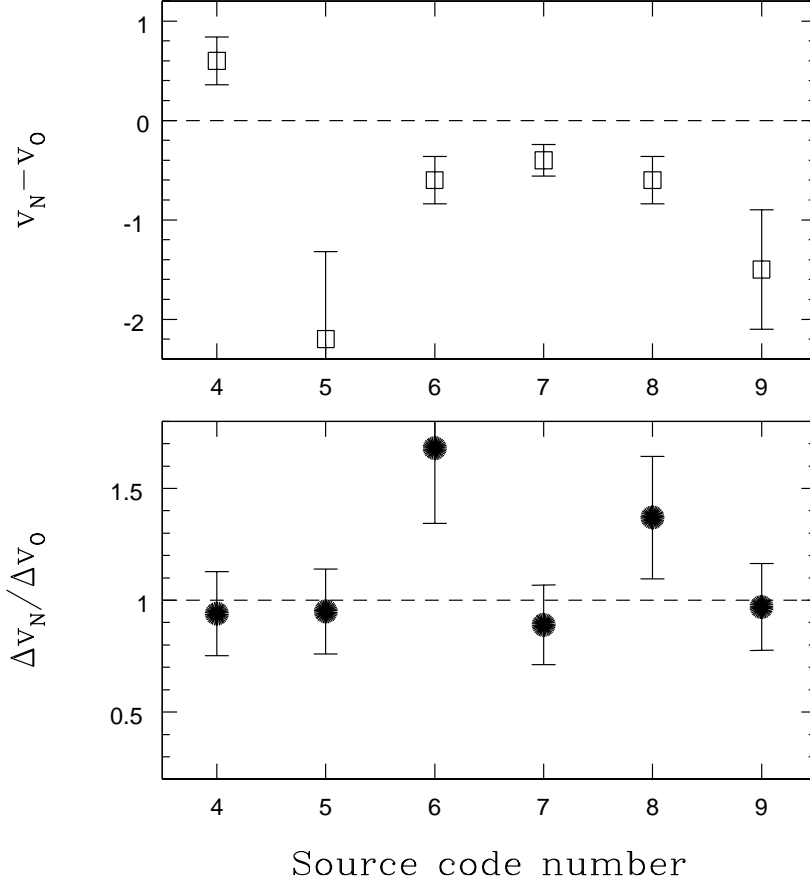


Fig. 6. Top panel: difference between the average velocities of unblended transitions of C_2H_5CN (V_N) and CH_3OCH_3 (V_O). Bottom panel: ratio between the average line widths at half maximum of C_2H_5CN (ΔV_N) and CH_3OCH_3 (ΔV_O). Source code number is taken from Table 1.

methanol and protonated methanol (Garrod & Herbst 2006), but both formation processes are not expected to involve species containing nitrogen. Furthermore, Bisschop et al. (2007) have indeed shown that in their HMCs the CH_3OCH_3 abundance does not correlate with that of other N-bearing species (see their Table 8). Nevertheless, based on considerations about abundance ratios and temperatures, they suggest that the O- and N-bearing molecules observed in their work may have experienced a common formation scheme.

In Figure 8 we plot the molecular abundances against the total H_2 column densities. Even though the uncertainties on these quantities are large, Figure 8 shows that on average cores with higher H_2 column density have also larger column densities of C_2H_5CN , C_2H_3CN and CH_3OCH_3 , without any substantial difference between O- and N-bearing species. We have also checked if a correlation is present between the observed abundances and the gas temperature: none of the sources show a correlation between these two parameters. In summary, we do not see

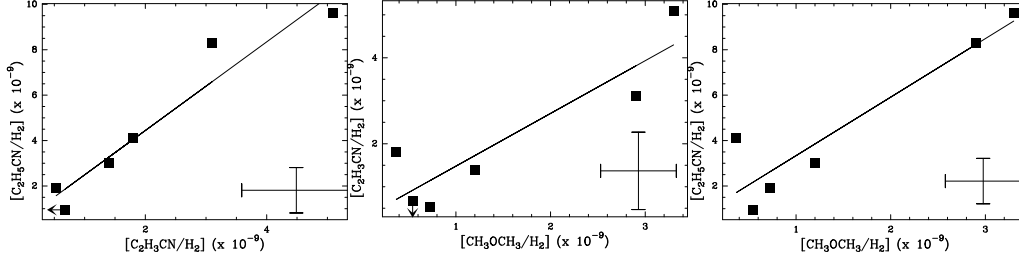


Fig. 7. Comparison between the molecular abundances of $\text{C}_2\text{H}_5\text{CN}$ and $\text{C}_2\text{H}_3\text{CN}$ (left panel), $\text{C}_2\text{H}_3\text{CN}$ and CH_3OCH_3 (central panel) and $\text{C}_2\text{H}_5\text{CN}$ and CH_3OCH_3 (right panel). All abundances are relative to H_2 . The solid lines correspond to the best-fits. The upper limit for the $\text{C}_2\text{H}_3\text{CN}$ abundance in G10.62 is indicated by an arrow. Errorbars representing the typical uncertainties are shown in the lower right corners.

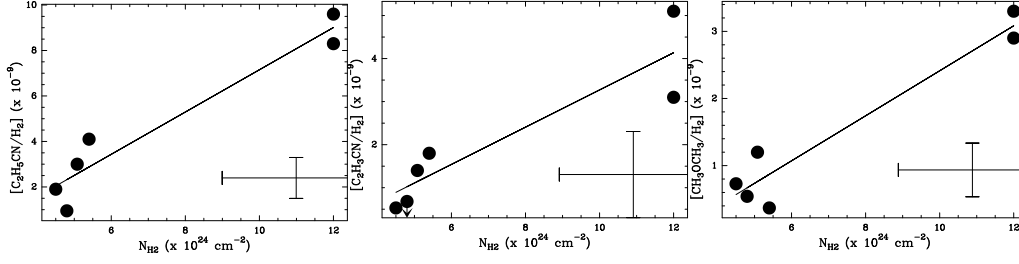


Fig. 8. Comparison between the H_2 total column density and the molecular abundances of $\text{C}_2\text{H}_5\text{CN}$ (left panel), $\text{C}_2\text{H}_3\text{CN}$ (central panel) and CH_3OCH_3 (right panel). The upper limit for the $\text{C}_2\text{H}_3\text{CN}$ abundance in G10.62 is indicated by an arrow. Errorbars representing the typical uncertainties are shown in the lower right corners.

any difference between CH_3OCH_3 and the two N-bearing species when comparing their abundances both to the gas temperature and density of the cores.

4.1.3. Beam-averaged column densities and rotational temperatures

Figure 9 shows the ratios between the beam averaged column densities (top panel) and those between the rotational temperatures derived from $\text{C}_2\text{H}_5\text{CN}$ and CH_3OCH_3 (see Tab. 4). The plot indicates that the column densities obtained from $\text{C}_2\text{H}_5\text{CN}$ are on average marginally higher (a factor of ~ 2.5) than those derived from CH_3OCH_3 , suggesting that $\text{C}_2\text{H}_5\text{CN}$ may indeed trace a region marginally denser than that traced by CH_3OCH_3 . We note a significant (a factor of ~ 11) difference in G19.61, which is the source in which there is also the largest difference in linewidths between $\text{C}_2\text{H}_5\text{CN}$ and CH_3OCH_3 , suggesting that $\text{C}_2\text{H}_5\text{CN}$ is actually associated with a denser and more turbulent sub-region of the HMC. On the other hand, no systematic difference is found in the rotational temperatures, with the significant exception of G10.62, for which we find a value more than 5 times higher from $\text{C}_2\text{H}_5\text{CN}$. However, for this source the temperature from CH_3OCH_3 is less accurate because it is derived from three transitions only.

Figs. 6, 7 and 9 do not allow to conclude that the O- and N-bearing species observed in this work trace different HMC regions. However, when discussing these results one has to bear in mind that the angular resolution of our data is much larger than the size of the HMC. High angular resolution observations have demonstrated that the environment of some of our HMCs, and in general of massive YSOs, has a complex structure, and may be fragmented in objects with different masses and in different evolutionary stages (see e.g. Garay et al. 1998 for G19.61; Avalos et al. 2006 and Mookerjee et al. 2007 for G34.26), whose angular separation is comparable to or even smaller than the angular resolution of the observations. The observed emission is hence affected both by the emission of other molecular condensations close to the main one and, less likely, by the emission of the cooler molecular gas of the envelope surrounding the HMC. Therefore, it is difficult to reveal a clear differentiation between O- and N-bearing species since the observed line parameters represent *average* values in the whole source.

Table 7: Line velocities (V_{LSR}) and widths at half maximum (ΔV) derived from single Gaussian fits to unblended lines for the sources G10.47, G10.62 and G19.61. The errors of the Gaussian fits to the lines are given between brackets.

Molecule	frequency (MHz)	V_{LSR} (km s ⁻¹)	ΔV (km s ⁻¹)
G10.47			
C ₂ H ₅ CN	98701.1090	67.249 (0.15)	8.411 (0.36)
	161581.2030	66.782 (0.48)	13.001 (1.37)
	161367.344	67.564 (0.37)	9.842 (0.86)
	224458.8590	66.546 (0.26)	10.180 (0.73)
	224419.8120	66.952 (0.35)	11.136 (1.12)
C ₂ H ₃ CN	147561.719	66.866 (0.49)	9.277 (1.20)
CH ₃ OCH ₃	111783.241	66.745 (0.14)	9.939 (0.36)
	111782.596	66.754 (0.14)	9.555 (0.22)
	147456.863	66.940 (0.54)	13.100 (1.19)
	237620.371	65.184 (0.43)	11.751 (1.07)
G10.62			
C ₂ H ₅ CN	161581.203	-1.667 (0.82)	5.934 (1.51)
	224045.750	0.395 (0.35)	4.703 (0.78)
	224419.812	-1.409 (0.40)	6.208 (0.83)
C ₂ H ₃ CN	—	—	—
CH ₃ OCH ₃	111783.241	-3.440 (0.28)	7.852 (0.58)
	111782.596	-3.429 (0.28)	7.357 (0.38)
	147210.732	-2.726 (0.27)	2.730 (0.57)

	237620.371	-2.615 (0.54)	5.690 (1.01)
<hr/>			
G19.61			
C ₂ H ₅ CN	98701.109	39.665 (0.40)	10.119 (0.95)
	161581.203	40.198 (0.52)	12.758 (1.57)
	161367.344	43.908 (0.72)	9.451 (2.02)
	224045.750	39.835 (0.43)	6.861 (1.06)
	224419.812	40.334 (0.39)	7.634 (1.25)
C ₂ H ₃ CN	–	–	–
CH ₃ OCH ₃	111783.241	41.429 (0.53)	5.955 (0.99)
	111782.596	41.427 (0.53)	5.264 (0.66)
<hr/>			
G29.96			
C ₂ H ₅ CN	98701.109	97.792 (0.29)	4.721 (0.91)
	161581.203	97.413 (0.73)	7.728 (2.19)
	161367.344	98.110 (1.47)	11.032 (4.69)
	224045.750	98.124 (0.73)	6.617 (1.53)
	224419.812	97.169 (0.24)	2.854 (0.59)
	224458.859	96.595 (0.60)	5.633 (1.39)
C ₂ H ₃ CN	–	–	–
CH ₃ OCH ₃	111783.241	97.929 (0.34)	5.675 (0.88)
	111782.596	97.976 (0.32)	4.919 (0.58)
	147210.732	105.190 (1.13)	10.947 (3.52)
<hr/>			
G31.41			
C ₂ H ₅ CN	98701.109	97.711 (0.26)	8.289 (0.58)
	161581.203	97.179 (0.38)	8.365 (1.07)
	161367.344	97.006 (1.02)	8.245 (2.25)
	224458.859	96.673 (0.50)	9.998 (1.67)
	224419.812	97.140 (0.36)	9.065 (0.93)
C ₂ H ₃ CN	147561.719	97.316 (0.46)	9.643 (1.10)
CH ₃ OCH ₃	111783.241	98.104 (0.06)	7.181 (0.15)
	111782.596	98.125 (0.06)	6.617 (0.10)
	147210.732	97.580 (0.18)	5.502 (0.49)
	173293.064	98.255 (0.36)	5.641 (0.83)
	237620.371	96.334 (0.20)	7.338 (0.46)
<hr/>			
G34.26			
C ₂ H ₅ CN	98701.109	57.333 (0.26)	7.449 (0.66)
	161581.203	57.511 (0.34)	8.542 (0.93)
	161367.344	57.103 (0.53)	8.368 (1.46)
	224045.750	57.610 (0.39)	3.691 (0.92)

	224419.812	57.478 (0.34)	6.052 (0.81)
C ₂ H ₃ CN	–	–	–
CH ₃ OCH ₃	111783.241	59.091 (0.11)	7.629 (0.25)
	111782.596	59.107 (0.10)	7.117 (0.16)
	147210.732	59.653 (0.35)	6.181 (0.84)
	173293.064	58.985 (0.27)	6.262 (0.72)
	237620.371	57.523 (0.17)	7.674 (0.38)

Table 8. Average line velocities and widths computed from the unblended lines of C₂H₅CN (V_N and ΔV_N , respectively) and CH₃OCH₃ (V_O and ΔV_O , respectively). Velocity differences ($V_N - V_O$) and linewidth ratios ($\Delta V_N / \Delta V_O$) are also given.

Source	V_N	V_O	$V_N - V_O$	ΔV_N	ΔV_O	$\Delta V_N / \Delta V_O$
	(km s ⁻¹)					
G10.47	67.0	66.4	0.6	10.5	11.1	0.94
G10.62	-0.9	-3.1	-2.2	5.6	5.9	0.95
G19.61	40.8	41.4	-0.6	9.4	5.6	1.68
G29.96	97.5	97.9	-0.4	6.4	7.2	0.89
G31.41	97.1	97.7	-0.6	8.9	6.5	1.37
G34.26	57.4	58.9	-1.5	6.8	7.0	0.97

4.2. Hot core chemical ages

When comparing the observed abundance of different molecular species (see Sect. 3.2) from predictions of theoretical models, we can get some insights into the evolutionary stage of HMCs.

H-rich species are thought to form in icy mantles of dust grains and then released into the gas phase when the central massive (proto)star begins to heat up the surroundings. A following gas phase chemistry transforms many of the grain mantle products into other species. In particular, C₂H₅CN, formed onto dust grains and then evaporated, is expected to form C₂H₃CN through gas-phase reactions (Caselli et al. 1993). The occurrence of these reactions, as well as those which destroy C₂H₃CN, depends on the core physical parameters, which are thought to change with the core evolution. Therefore, the abundance ratio of C₂H₅CN and C₂H₃CN is correlated to the core evolutionary stage, and can be used as a ‘chemical clock’ for the HMC.

In Col. 2 of Tab. 9 we list the observational values for the abundance ratio $R = X(\text{C}_2\text{H}_3\text{CN})/X(\text{C}_2\text{H}_5\text{CN})$, derived from the molecule’s abundances given in Col. 6 of Table 4. We also plot these ratios in Fig. 10 together with the predictions of the chemical models of Caselli et al. (1993) for the Orion-HC and Compact Ridge. The physical and chemical properties of these two regions can be considered as ‘extrema’ for our HMCs, so that we will use them to constrain

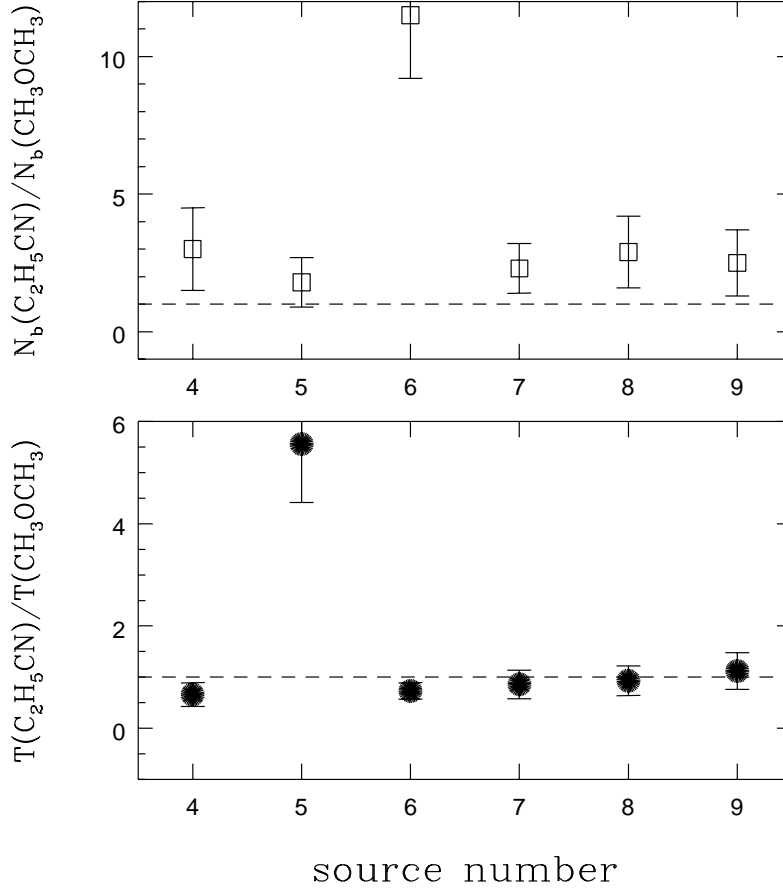


Fig. 9. Top panel: ratio between the beam averaged total column densities (N_b in Tab. 4) derived from $\text{C}_2\text{H}_5\text{CN}$ and CH_3OCH_3 . Bottom panel: ratio between the rotational temperatures derived from $\text{C}_2\text{H}_5\text{CN}$ and CH_3OCH_3 . The numbers on the x-axis indicate the identification number of each source as in Tab. 1. The dashed line represents equal column density or rotational temperature from $\text{C}_2\text{H}_5\text{CN}$ and CH_3OCH_3 .

the chemical ages of our sample. Chemical models predict a sharp decrease in the abundances of many complex molecules, among which are $\text{C}_2\text{H}_3\text{CN}$ and $\text{C}_2\text{H}_5\text{CN}$, in HMCs after $\sim 10^5$ yrs (see Fig. 10). Therefore, the detection of several lines of both $\text{C}_2\text{H}_3\text{CN}$ and $\text{C}_2\text{H}_5\text{CN}$ suggest that all of our HMCs are likely younger than $\sim 10^5$ yrs. In fact, we find ages in the range from $\sim 3.7 \times 10^4$ to $\sim 5.9 \times 10^4$ yrs, with the HMC in G34.26 being the youngest and that in G29.96 the oldest. We point out that this procedure does not take into account the errors in the model predictions.

In Fig. 11 we also plot R against the $\text{C}_2\text{H}_5\text{CN}$ fractional abundance and we compare it with the theoretical curve predicted for the Orion HC. From Fig. 11 we deduce that the model underestimates the observed ratio by a factor greater than 10. This could be due to a missing reaction

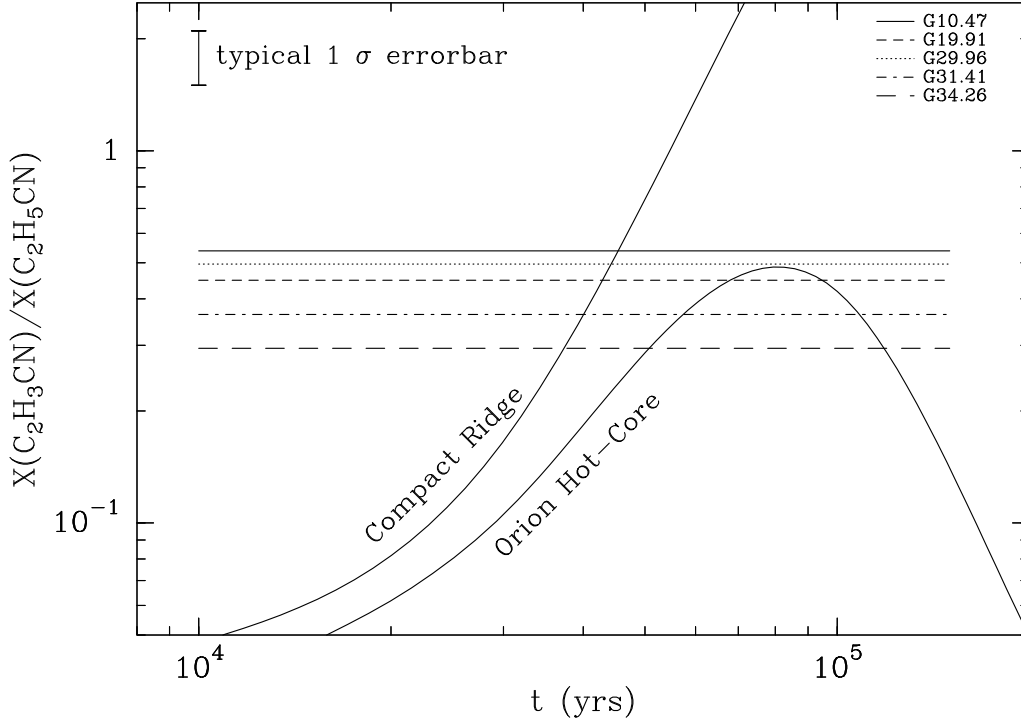


Fig. 10. Comparison between the observed abundance ratio of the daughter/parent pair C_2H_3CN/C_2H_5CN and the predictions of the chemical models of Caselli et al (1993). The observed abundance ratio of each source is plotted as a horizontal line (see the top right corner for the source identification). The curves correspond to the predictions of the models by Caselli et al. (1993) for the Orion-HC (corresponding to $T = 200$ K and $n_{H_2} = 10^7 \text{ cm}^{-3}$) and Compact Ridge (corresponding to $T = 100$ K and $n_{H_2} = 10^6 \text{ cm}^{-3}$).

in the chemical network between C_2H_5CN and H_3O^+ . In fact, the hydronium ion is quite abundant in the HMC phase and could destroy some of the C_2H_5CN molecules, thus increasing the observed C_2H_3CN/C_2H_5CN abundance ratio (see e.g. Caselli et al. 1993). Another possibility is that additional C_2H_3CN forms in gas phase reactions as suggested by Charnley et al. (1992) and Rodgers & Charnley (2001).

4.3. Comments on individual sources

In this Section we describe the main properties of each source on the basis of the results obtained both in this work and from previous observations.

G10.47+0.03 In this region three UC HII's are associated with a HMC (see e.g. Gibb et al. 2004). Observations of CH_3CN (13–12) and (19–18) (Hatchell et al. 1998) show that the temperature increases from ~ 87 K at a distance of $\sim 2.3''$ from the centre, to ~ 134 K at $0.8''$ from the centre, indicating a temperature gradient. This is confirmed by observations of the NH_3 (4,4) inversion transition (Cesaroni et al. 1998), that show temperature and velocity gradients, which can be interpreted in terms of a rotating structure with temperature increasing towards the centre. Our

Table 9. Hot cores chemical ages

Source	R	t_{min}	t_{max}
		$(\times 10^4 \text{ yr})$	
G10.47	0.5 ± 0.2	5.0	5.4
G19.61	0.4 ± 0.2	4.7	5.0
G29.96	0.5 ± 0.1	4.7	5.9
G31.41	0.4 ± 0.1	4.3	4.7
G34.26	0.3 ± 0.1	3.7	4.2

$$R = X(\text{C}_2\text{H}_3\text{CN})/X(\text{C}_2\text{H}_5\text{CN})$$

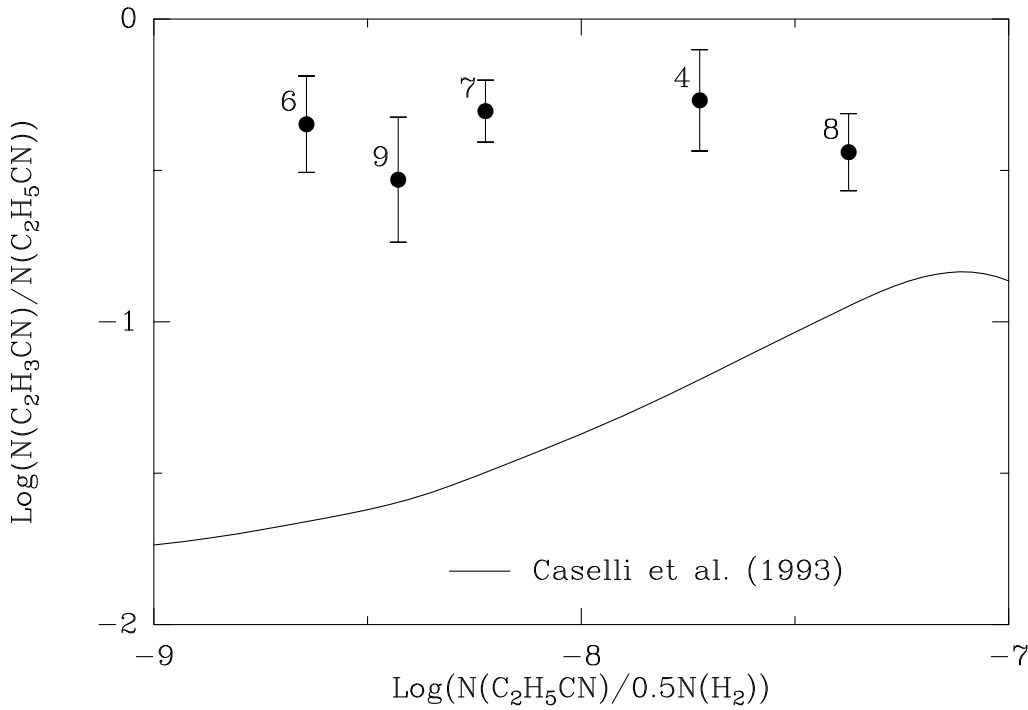


Fig. 11. Observed abundance ratio $R = X(\text{C}_2\text{H}_3\text{CN})/X(\text{C}_2\text{H}_5\text{CN})$ against $\text{C}_2\text{H}_5\text{CN}$ fractional abundance. The solid line represents the prediction of the model by Caselli et al. (1993) for the Orion-HC ($T = 200 \text{ K}$, $n = 10^7 \text{ cm}^{-3}$). The numbers identify the sources as in Table 1.

temperature measurements agree with the estimates obtained by Hatchell et al. (1998) at $\sim 1''$ from the core centre.

Fig. 6 indicates a small difference in the line velocities of O- and N-bearing molecules, suggesting that they are likely arising from marginally different regions. This result agrees with that of Olmi et al. (1996), who found a displacement between HCOOCH_3 and CH_3CN of $\sim 0.5''$. The most surprising property of this source is the high $\text{C}_2\text{H}_3\text{CN}$ column density. The presence of both vibrationally excited (see Sect. 3.4) and "weak" b-type lines (see Sect. 3.2.4) suggest that

$\text{C}_2\text{H}_3\text{CN}$ is about 10 times more abundant than $\text{C}_2\text{H}_5\text{CN}$. If we use in the rotation diagram all our data ("strong", "weak" and vibrationally excited lines) and we correct for the optical depth (see Wyrowski et al. 1999 for the procedure) we obtain the following best fit parameters: $N_s \sim 1.7 \times 10^{18} \text{ cm}^{-2}$, $T_{\text{rot}} \sim 140 \text{ K}$ and $\theta \sim 1''$. A previous study of vibrationally excited HC_3N also showed anomalous high abundance for this molecule, a column density of $\sim 4 \times 10^{18} \text{ cm}^{-2}$, comparable with that from $\text{C}_2\text{H}_3\text{CN}$. This result is in agreement with the model predictions of Caselli et al. (1993), who showed that the abundances of HC_3N and $\text{C}_2\text{H}_3\text{CN}$, after evaporation from dust grains, vary in a very similar way both in the Orion-HC for $t > 100 \text{ yrs}$ (see their Fig. 4) and in the Compact Ridge for $t \geq 10^4 \text{ yrs}$ (see their Fig. 5), while those of $\text{C}_2\text{H}_5\text{CN}$ and HC_3N are very different between them. In fact, the destruction of $\text{C}_2\text{H}_5\text{CN}$ by molecular ions (in particular H_3^+) leads to the production of both $\text{C}_2\text{H}_3\text{CN}$ and HC_3N via dissociative recombination of $\text{C}_3\text{H}_4\text{N}^+$ (formed in the reaction with H_3^+).

G10.62–0.38 This star forming region consists of a cluster of OB stars embedded in a dense, collapsing molecular cloud (Ho & Haschick 1986, Keto et al. 1987, 1988, Sollins et al. 2005). Keto et al. (1987) find an average temperature of 95 K for the absorption components at -3.0 and -0.5 km s^{-1} and 140 K at 1.9 km s^{-1} , while the average temperature for the gas seen in emission, away from the UC HII, is 54 K: they suggest a temperature decreasing from the HMC center with a power-law of the type $R^{-0.5}$. The temperature derived from $\text{C}_2\text{H}_5\text{CN}$ (see Tab. 4) indicates that this molecule traces a region at about 0.1 pc from the centre of the core, which also coincides with the centre of the continuum emission of the UC HII region. The $\text{C}_2\text{H}_5\text{CN}$ and CH_3OCH_3 line velocities in Fig. 6 show that these molecules are spatially separated, with the latter more distant from the UC HII. This is also suggested by the temperature derived from CH_3OCH_3 , even though the statistics are very poor because only three lines at $E_u < 100 \text{ K}$ have been identified. We find only one blended transition of $\text{C}_2\text{H}_3\text{CN}$ in all our spectra so we cannot estimate rotational temperature and column density for this molecule.

G19.61–0.23 This is a complex region with an irregular structure both of the ionized gas (Wood & Churchwell 1990), and of the molecular emission from the associated molecular clumps. Garay et al. (1998) found five distinct UC HII regions excited by individual stars from VLA observations of the ionized and molecular gas ($\text{NH}_3(2,2)$ inversion line): the cometary-like and most compact of them is associated with the densest ammonia clump, called Middle clump to distinguish it from the Northern and the Southwestern clumps. The Middle clump exhibits very broad line widths ($\sim 9.5 \text{ km s}^{-1}$) and is characterized by a V_{LSR} of $39.3 \pm 0.1 \text{ km s}^{-1}$ in the main $\text{NH}_3(2,2)$ line: these values are similar to those we find for $\text{C}_2\text{H}_5\text{CN}$. The Southwestern clump shows lower ΔV and higher V_{LSR} equal to those for CH_3OCH_3 . This seems to suggest that N- and O-bearing molecular emission originates from separate regions. This is confirmed by the column density ratio between $\text{C}_2\text{H}_5\text{CN}$ and CH_3OCH_3 , much higher than those of the other sources (see Fig. 9), suggesting that $\text{C}_2\text{H}_5\text{CN}$ indeed traces a region denser than that traced by O-bearing species.

In spite of this, high angular resolution observations of two rotational lines of $\text{C}_2\text{H}_5\text{CN}$ and HCOOCH_3 , performed with BIMA (Remijan et al. 2004), indicate that these molecules seem to trace the same region.

G29.96–0.02 G29.96 is an example of UC HII cometary region. High angular resolution VLA observations in the ammonia (4,4) inversion transition (Cesaroni et al. 1998) show that the HMC has a nearly symmetric profile, and is not affected by the presence of the embedded UC HII region. Our rotational temperatures agree with those obtained by Hatchell et al. (1998) from CH_3CN (13–12) and (19–18) and are higher than the estimate that they derive from CH_3OH ($T_{\text{rot}} \sim 48$ K). This could indicate that O-bearing molecules map colder and extended gas. Nevertheless, Fig. 6 does not show any displacement between the location of O- and N-bearing molecules: both their ΔV and V_{LSR} are, in fact, equal within the error bars. This is supported by high angular resolution observations (Olmi et al. 2003) which have shown that some lines of HCOOCH_3 and the N-bearing molecule CH_3CN trace approximately the same region. Our V_{LSR} also agrees with those of C^{17}O (2-1) and (3-2) measured by Hofner et al. (2000).

G31.41+0.31 The region is made of a core-halo UC HII region, offset by $\sim 5''$ from a hot core in which Beltrán et al. (2005) have revealed a rotating toroidal structure. Also, as already mentioned in Sect. 3.1, they serendipitously detected the $\text{C}_2\text{H}_5\text{CN}$ ($25_{2,24} - 24_{2,23}$) and $\text{HCOOCH}_3\text{-A}$ ($25_{11,15} - 26_{9,18}$) lines, and found from their high-angular resolution maps that, even though the two tracers peak at slightly different positions, their integrated emissions and that of the 1.4 mm continuum are fairly well overlapping. Interferometric observations of CH_3CN lines (Olmi et al. 1996; Beltrán et al. 2005) and of the NH_3 (4,4) main and satellite inversion lines (Cesaroni et al. 1998) show that both the column density and the temperature increase towards the HMC center. This hot and dense gas has also been detected through HC_3N (17-16) in its v_7 and v_6 vibrationally excited states (Wyrowski et al. 1999). The ratio between the intensity of these two lines point to temperatures of ~ 250 K.

Lower angular resolution maps of the CH_3CN (19-18) and (13-12) transitions (Hatchell et al. 1998) give a temperature in agreement with the estimate that we derive from our molecules (see Tab. 4). The ΔV of the CH_3CN lines are comparable to those measured by us from $\text{C}_2\text{H}_5\text{CN}$. CH_3OCH_3 and HCOOCH_3 have lower ΔV , but the difference in V_{LSR} between the O- and N-bearing molecules is small.

G34.26+0.15 This is a complex massive star formation region located at a distance of 3.7 kpc (Kuchar & Bania 1994) extensively studied both in radio continuum (Wood & Churchwell 1989; Avalos et al. 2006) and in molecular lines (e.g. Garay & Rodríguez 1990; Hatchell et al. 1998; Sewilo et al. 2004). VLA observations of the NH_3 (2,2) and (3,3) inversion transitions (Garay & Rodríguez 1990) reveal the presence of three distinct regions of the molecular gas:

- a low density ($n(\text{H}_2) \approx 10^4 \text{ cm}^{-3}$), low-temperature ($T_{\text{rot}} \approx 18 \text{ K}$) gas in front of a bright cometary UC HII region.
- a warm gas ($T_{\text{rot}} \approx 70 \text{ K}$) in a molecular disk-like structure $\approx 7.3'' \times 2.8''$ in size, mapped by the main hyperfine component of the (3,3) transition, seen in absorption.
- an ultracompact region $\approx 1.6''$ in size, $\approx 2''$ to the east of the bright cometary UC HII region, traced by the satellite hyperfine lines of the (2,2) and (3,3) transitions. It is characterized by a rotational temperature of $185^{+75}_{-45} \text{ K}$ and by a H_2 density of $\approx 7 \times 10^7 \text{ cm}^{-3}$.

The H_2 density and temperatures estimated from the tracers studied in this paper agree with those given by Garay & Rodríguez (1990). Mookerjee et al. (2007) have observed with $\sim 1''$ resolution two transitions of $\text{C}_2\text{H}_5\text{CN}$, and one transition of CH_3OCH_3 and HCOOCH_3 , but all of them fall out of the bands observed in this work. From these maps and those of other molecular species, Mookerjee et al. (2007) have concluded that O- and N-bearing species peak at different positions, separated by $\sim 0''.8$, with a spatial separation similar to that observed in Orion. Given the low angular resolution of our data and the complexity of the region, such a differentiation is not shown from our observations. Hatchell et al. (1998) found evidence for temperature and density gradient in this source: the high excitation CH_3CN (19-18) transitions trace a smaller, hotter and denser region than that traced by CH_3CN (13-12). Our $\text{C}_2\text{H}_5\text{CN}$ and CH_3OCH_3 temperatures agree with those of the higher excitation lines, indicating that they trace the same hot gas.

5. Conclusions

We have surveyed rotational transitions of 4 complex O- and N-bearing molecules, $\text{C}_2\text{H}_3\text{CN}$, $\text{C}_2\text{H}_5\text{CN}$, CH_3OCH_3 and HCOOCH_3 , with the IRAM-30m telescope towards a selected sample of 12 well-known HCs, all of them associated with UC HII regions. For 6 sources of our sample, we have detected a sufficient number of transitions to derive the main physical properties of the cores. We focus our analysis on the 3 species $\text{C}_2\text{H}_3\text{CN}$, $\text{C}_2\text{H}_5\text{CN}$ and CH_3OCH_3 only, because the HCOOCH_3 lines are usually blended. The main results of our study are summarised as follows:

- From the rotational lines of $\text{C}_2\text{H}_3\text{CN}$, $\text{C}_2\text{H}_5\text{CN}$ and CH_3OCH_3 , we have derived rotational temperatures from ~ 100 to $\sim 150 \text{ K}$, and source averaged total column densities of order of $10^{15} - 10^{17} \text{ cm}^{-2}$. Temperatures and column densities derived from the three tracers are typically in good agreement among them in each source, indicating that they are tracing approximately the same dense and hot gas of the cores.
- The abundances relative to H_2 are of the order of $\sim 10^{-9} - 10^{-10}$ for all species, and are comparable to the values found in the Orion-hot core and in Sgr B2. The $\text{C}_2\text{H}_5\text{CN}$ abundances are also comparable to those derived in other HMCs by Bisschop et al. (2007), while for CH_3OCH_3 we find values a factor of ~ 2.5 lower. There is a strong correlation between the abundances of $\text{C}_2\text{H}_5\text{CN}$ and $\text{C}_2\text{H}_3\text{CN}$, as expected from theory that predicts that the latter is formed through gas phase reactions involving $\text{C}_2\text{H}_5\text{CN}$. Interestingly, a correlation is present

also between the two N-bearing species and CH_3OCH_3 , in disagreement with the results found by Bisschop et al. (2007) in similar sources.

- Single Gaussian fits to unblended lines reveal a small difference between the average peak velocity of $\text{C}_2\text{H}_5\text{CN}$ and CH_3OCH_3 lines, suggesting a possible spatial separation of the two tracers, as seen in Orion and W3(H_2O). On the other hand, no systematic differences are found in the linewidths. We find a clear difference only in G19.61. We believe that this partly is due to the poor angular resolution of our observations, which allows us to derive only average values over the sources, which show a complex morphology.
- We have compared the abundance ratio of the daughter/parent pair $\text{C}_2\text{H}_5\text{CN}/\text{C}_2\text{H}_3\text{CN}$ with the predictions of chemical models to constrain the HCs' chemical ages. We find ages between $3.7\text{--}5.9 \times 10^4$ yrs. We also compared this ratio against $\text{C}_2\text{H}_5\text{CN}$ fractional abundance, finding that chemical models underestimate even by a factor greater than 10 our observational results.

The chemical and physical differentiation between O- and N-bearing molecules seen in the Orion HC and W3(H_2O) is not revealed by our observations of other HMCs. We stress however that our data have beam size much larger than the diameters of the HMCs, providing only *average* values of the physical parameters of interest in the whole molecular clump hosting the cores, and may be affected by other objects embedded inside the clumps themselves. Follow-up observations with millimeter and sub-millimeter interferometers (in particular ALMA, available in the near future) will be fundamental to provide maps with resolution comparable or even smaller than the core sizes, thus allowing us to derive with better spatial accuracy the physical parameters of the HMCs.

Acknowledgements. We are grateful to the IRAM-30m telescope staff for their assistance. We thank Peter Schilke for providing us with the XCLASS program. Ilaria Pascucci would like to thank Thomas Henning for helpful discussions. Many thanks to Geoff Macdonald for his corrections and suggestions.

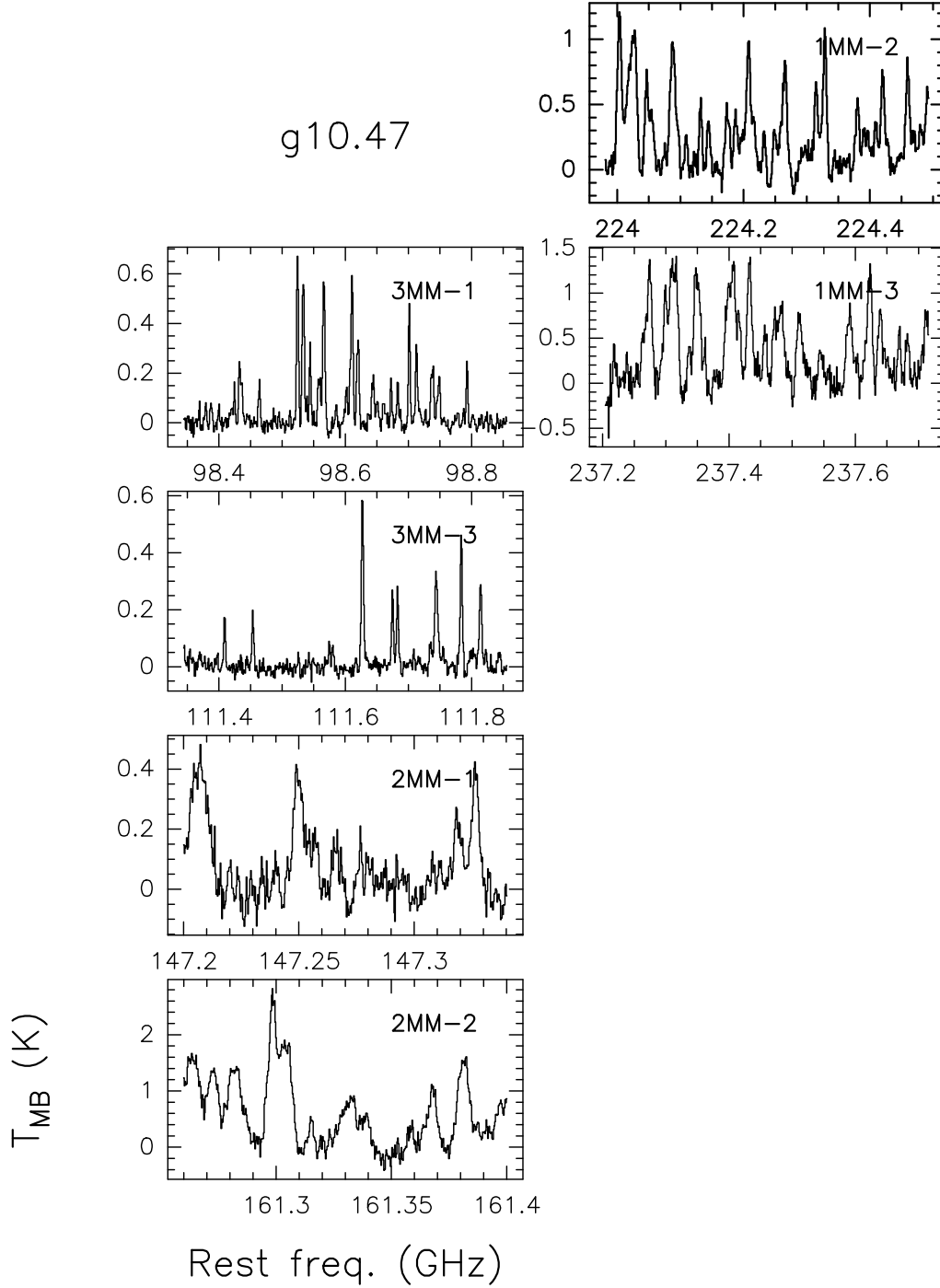


Fig. .1. Spectra obtained towards G10.47 with the IRAM-30m Telescope during the 1997 observing run.

Appendix A: Observed spectra

Appendix B: Tables

Tables .1–.11 list the molecular transitions used to derive the rotational temperatures and total column densities of the sources in Table 3. For each line we give: rest frequency, ν , in MHz (Col. 1, indicated with "b" if it is a b-type transition); the molecular species (Col. 2); the energy

g10.47

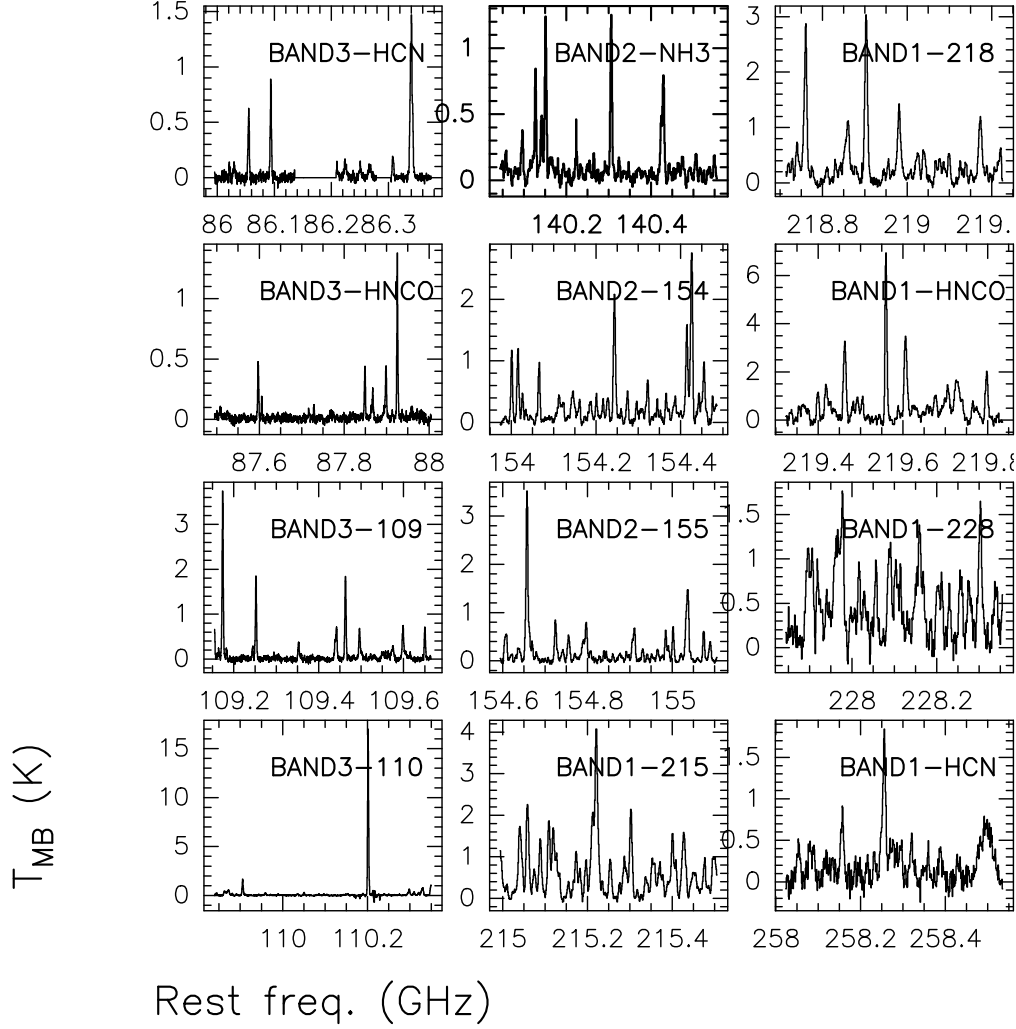


Fig. .2. Spectra obtained towards G10.47 with the IRAM-30m Telescope during the 1996 observing run.

of the lower level, E_l , in cm^{-1} (Col. 3); the line integrated emission, $\int T_{MB} dv$, in K km s^{-1} ; (Col. 4); the quantity $\mu^2 S$, where μ (in Debye) is the molecule's dipole moment and S is the line strength (Col. 5). The CH_3OCH_3 lines are separated in four components not resolved in our spectra (see also Sect. 4.1). For this reason, for the CH_3OCH_3 transitions we give in Col. 4 the total integrated emission of the four components divided by the sum of the statistical weights of each component (for the statistical weights see Groner et al. 1998).

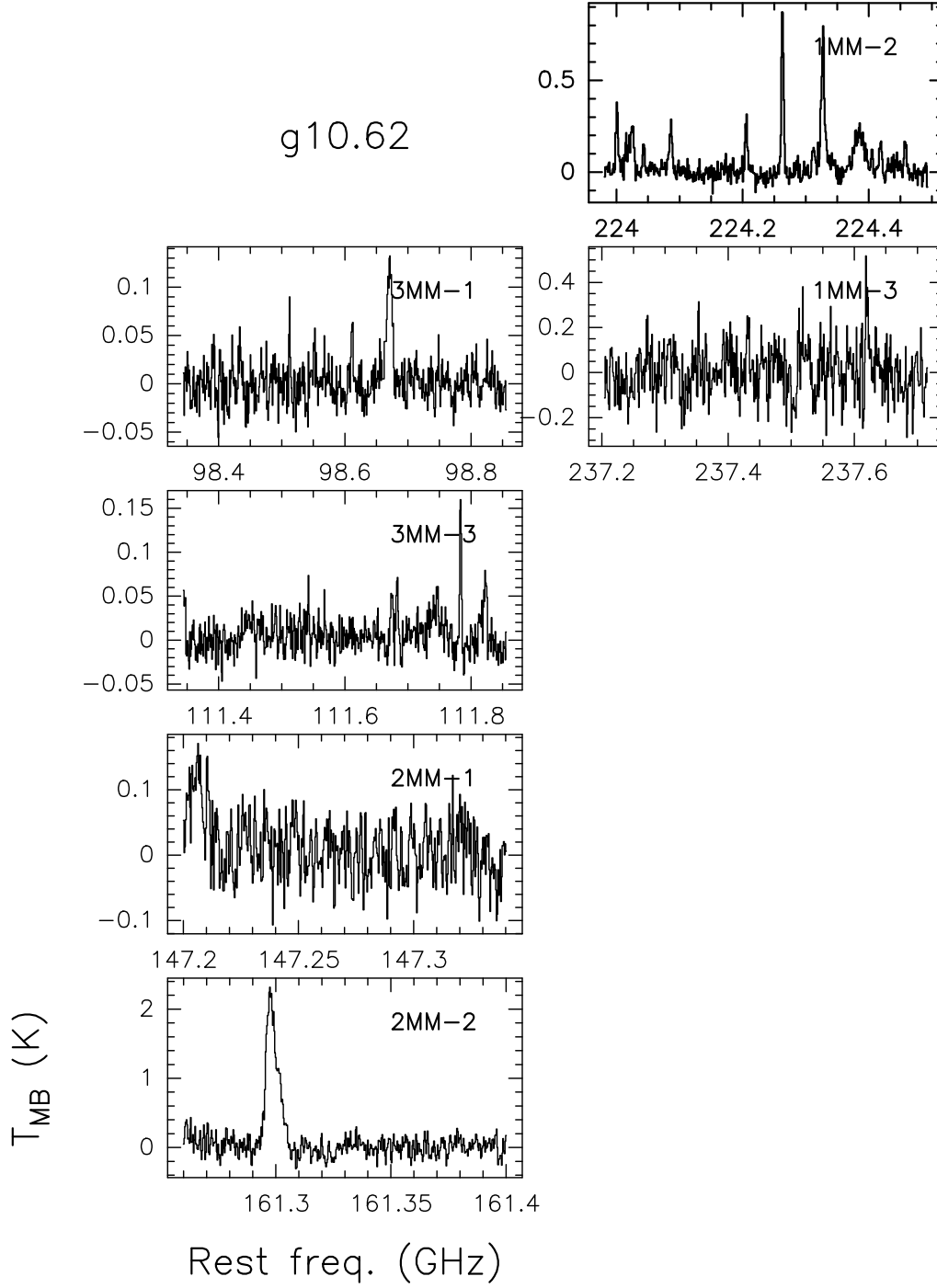


Fig. .3. Same as Fig. .1 for G10.62.

Table .1: Transitions observed towards G10.47 during the 1997 observing run.

ν (MHz)	Molecule	E_l (cm ⁻¹)	$\int T_{MB} d\nu$ (K km s ⁻¹)	$\mu^2 S$ (D ²)
b98399.6170	C ₂ H ₃ CN	66.0140	0.498	4.682

98523.883	C ₂ H ₅ CN	44.251	3.33	113.939
98524.664	C ₂ H ₅ CN	54.287	3.05	96.525
98532.070	C ₂ H ₅ CN	65.860	3.19	76.412
98533.9845	C ₂ H ₅ CN	35.754	4.16	128.685
98544.148	C ₂ H ₅ CN	78.967	2.78	53.615
98559.867	C ₂ H ₅ CN	93.604	1.64	28.149
98564.836	C ₂ H ₅ CN	28.801	4.11	140.761
98566.797	C ₂ H ₅ CN	28.801	3.15	140.761
98701.109	C ₂ H ₅ CN	23.398	4.38	150.140
b111574.6250	C ₂ H ₅ CN	73.7330	0.74	10.807
b111783.241	CH ₃ OCH ₃	17.550	0.1439	27.2197
b111802.549	CH ₃ OCH ₃	42.142	0.0287	4.43093
b111813.417	CH ₃ OCH ₃	118.013	0.1204	96.5637
b147205.839	CH ₃ OCH ₃	22.082	0.2271	19.52177
b147456.863	CH ₃ OCH ₃	257.141	0.1097	145.57157
147561.719	C ₂ H ₃ CN	38.4910	4.70	232.515
161261.141	C ₂ H ₅ CN	95.144	13.0	213.000
161265.734	C ₂ H ₅ CN	108.253	12.5	199.066
b161281.953	CH ₃ OCH ₃	75.305	0.3944	49.41313
161289.996	CH ₃ OCH ₃	333.668	0.1341	162.13361
161303.484	C ₂ H ₅ CN	139.060	9.28	166.301
161304.922	C ₂ H ₅ CN	73.536	11.3	235.930
161367.344	C ₂ H ₅ CN	175.957	9.38	126.974
161380.828	C ₂ H ₅ CN	101.33	15.13	246.2506
161397.047	C ₂ H ₃ CN	97.1140	6.92	217.164
161441.2660	C ₂ H ₃ CN	139.0100	5.87	386.26
161445.3910	C ₂ H ₃ CN	67.1130	7.04	234.339
161450.3590	C ₂ H ₃ CN	67.1130	7.04	234.339
161475.172	C ₂ H ₅ CN	52.712	19.70	258.004
161502.266	C ₂ H ₃ CN	56.6050	9.00	240.337
161516.7190	C ₂ H ₅ CN	58.1110	9.38	252.312
161527.500	C ₂ H ₃ CN	192.6770	5.77	162.238
161581.203	C ₂ H ₅ CN	58.115	14.3	252.312
161582.047	C ₂ H ₃ CN	223.8800	3.37	144.202
161643.250	C ₂ H ₃ CN	257.9690	4.50	124.459
224002.109	C ₂ H ₅ CN	166.828	4.40	309.672
224003.438	C ₂ H ₅ CN	152.185	6.00	320.879
224045.750	C ₂ H ₅ CN	200.696	5.73	283.720

224084.281	C ₂ H ₅ CN	219.912	5.20	268.960
224088.2035	C ₂ H ₅ CN	127.510	6.00	339.753
224131.516	C ₂ H ₅ CN	240.640	3.63	253.034
224186.344	C ₂ H ₅ CN	262.876	3.27	235.930
224206.609	C ₂ H ₅ CN	117.492	4.09	347.406
224208.078	C ₂ H ₅ CN	117.492	4.09	347.406
b224231.6880	C ₂ H ₅ CN	94.4160	2.05	33.527
224248.016	C ₂ H ₅ CN	286.614	2.21	217.645
224389.719	C ₂ H ₅ CN	338.567	2.25	177.537
224419.812	C ₂ H ₅ CN	109.033	6.34	353.894
224458.859	C ₂ H ₅ CN	109.036	8.10	353.894
b237360.8910	C ₂ H ₅ CN	114.9850	2.33	24.209
237396.9765	C ₂ H ₃ CN	168.5260	5.15	336.209
237405.1880	C ₂ H ₅ CN	101.8870	13.71	380.894
237456.2500	C ₂ H ₃ CN	216.3420	5.07	635.06
237482.766	C ₂ H ₃ CN	132.5690	4.06	350.218
237485.016	C ₂ H ₃ CN	132.5700	3.61	350.218
237548.541	CH ₃ OCH ₃	447.259	0.200	34.69413
237585.484	C ₂ H ₃ CN	275.8720	3.58	294.183
237591.391	C ₂ H ₃ CN	108.5880	6.11	359.528
b237620.371	CH ₃ OCH ₃	32.291	0.551	23.17836
237638.0160	C ₂ H ₃ CN	119.0860	6.74	355.471
237668.766	C ₂ H ₃ CN	309.9800	4.29	280.758

Table .2: Transitions observed towards G10.47 during the 1996 observing run.

ν (MHz)	Molecule	E_l (cm ⁻¹)	$\int T_{MB} dv$ (K km s ⁻¹)	$\mu^2 S$ (D ²)
b140163.0	CH ₃ OCH ₃	308.85	0.1086	23.138
b140226.172	CH ₃ OCH ₃	159.81	0.0911	9.896
a140429.484	C ₂ H ₃ CN	54.24	8.45	202.872
b154027.062	C ₂ H ₃ CN	10.02	4.68	2.344
a154724.531	C ₂ H ₃ CN	65.42	9.77	215.731
b154311.469	CH ₃ OCH ₃	185.5	0.0667	12.855
b154456.5	CH ₃ OCH ₃	62.92	0.4117	21.739
215040.8	C ₂ H ₅ CN	229.5	24.1	1199.4
215088.203	C ₂ H ₅ CN	288.76	15.5	533.6
215109.047	C ₂ H ₅ CN	183.46	19.7	651.1

215119.203	C ₂ H ₅ CN	135.84	16.5	369.7
215126.703	C ₂ H ₅ CN	316.4	10.0	502.8
215400.797	C ₂ H ₅ CN	156.87	17.6	340.3
215427.984	C ₂ H ₅ CN	156.88	19.0	340.332
227897.625	C ₂ H ₃ CN	242.47	13.12	594.744
227906.719	C ₂ H ₃ CN	214.46	10.29	609.457
227918.656	C ₂ H ₃ CN	274.75	9.18	577.798
227960.234	C ₂ H ₃ CN	311.27	7.23	558.56
227967.594	C ₂ H ₃ CN	190.74	19.11	621.8
228017.375	C ₂ H ₃ CN	352.	10.23	537.313
228087.297	C ₂ H ₃ CN	396.91	6.95	513.431
228090.531	C ₂ H ₃ CN	156.23	8.88	319.903
228104.609	C ₂ H ₃ CN	171.34	11.91	315.959
228160.297	C ₂ H ₃ CN	171.35	16.7	631.917

Table .3: Transitions observed towards G10.62–0.38 during the 1997 observing run.

ν (MHz)	Molecule	E_l (cm ⁻¹)	$\int T_{MB} d\nu$ (K km s ⁻¹)	$\mu^2 S$ (D ²)
b111783.241	CH ₃ OCH ₃	17.550	0.0403	27.2197
111802.17	CH ₃ OCH ₃	42.141	0.016	2.53886
111802.93	CH ₃ OCH ₃	42.142	0.013	2.53886
111813.417	CH ₃ OCH ₃	118.013	0.016	96.5637
b147205.839	CH ₃ OCH ₃	22.082	0.0478	19.52177
147456.863	CH ₃ OCH ₃	257.141	0.0196	145.57157
161261.141	C ₂ H ₅ CN	95.144	1.82	213.000
161265.734	C ₂ H ₅ CN	108.253	0.32	199.066
161281.953	CH ₃ OCH ₃	75.305	0.0572	49.41313
161289.996	CH ₃ OCH ₃	333.668	0.0572	162.13361
161475.172	C ₂ H ₅ CN	52.712	0.86	258.004
161581.203	C ₂ H ₅ CN	58.115	1.07	252.312
224002.109	C ₂ H ₅ CN	166.828	0.78	309.672
224003.438	C ₂ H ₅ CN	152.185	0.97	320.879
224045.750	C ₂ H ₅ CN	200.696	0.65	283.720
224084.281	C ₂ H ₅ CN	219.912	0.39	268.960
224088.2035	C ₂ H ₅ CN	127.510	1.16	339.753
224206.609	C ₂ H ₅ CN	117.492	1.05	347.406

224208.078	C ₂ H ₅ CN	117.492	0.67	347.406
224419.812	C ₂ H ₅ CN	109.033	1.20	353.894
224458.859	C ₂ H ₅ CN	109.036	1.05	353.894
237261.970	CH ₃ OCH ₃	214.188	0.117	66.88355
237548.541	CH ₃ OCH ₃	447.259	0.117	34.69413
b237620.371	CH ₃ OCH ₃	32.291	0.0875	23.17836

Table .4: Transitions observed towards G10.62–0.38 during the 1996 July observing run.

ν (MHz)	Molecule	E_l (cm ⁻¹)	$\int T_{MB} d\nu$ (K km s ⁻¹)	$\mu^2 S$ (D ²)
215040.8	C ₂ H ₅ CN	229.5	2.49	1199.4
215109.047	C ₂ H ₅ CN	183.46	3.25	651.1
215427.984	C ₂ H ₅ CN	156.88	1.67	340.332

Table .5: Transitions observed towards G19.61–0.23 during the 1997 observing run.

ν (MHz)	Molecule	E_l (cm ⁻¹)	$\int T_{MB} d\nu$ (K km s ⁻¹)	$\mu^2 S$ (D ²)
98523.883	C ₂ H ₅ CN	44.251	1.24	113.939
98524.664	C ₂ H ₅ CN	54.287	0.87	96.525
98532.070	C ₂ H ₅ CN	65.860	0.75	76.412
98533.9845	C ₂ H ₅ CN	35.754	1.49	128.685
98544.148	C ₂ H ₅ CN	78.967	0.69	53.615
98564.836	C ₂ H ₅ CN	28.801	1.21	140.761
98566.797	C ₂ H ₅ CN	28.801	0.72	140.761
98701.109	C ₂ H ₅ CN	23.398	1.24	150.140
b104177.000	CH ₃ OCH ₃	102.625	0.185	79.56847
104212.656	C ₂ H ₃ CN	23.4110	0.80	155.205
104419.312	C ₂ H ₃ CN	71.4640	0.80	112.653
104432.797	C ₂ H ₃ CN	30.9450	0.72	148.58
104437.516	C ₂ H ₃ CN	90.9290	0.94	95.507
104453.930	C ₂ H ₃ CN	30.9460	0.72	148.58
104490.168	CH ₃ OCH ₃	585.600	0.026	4.48006
b111783.241	CH ₃ OCH ₃	17.550	0.017	27.2197
b111813.417	CH ₃ OCH ₃	118.013	0.024	96.5637

147205.839	CH ₃ OCH ₃	22.082	0.0376	19.52177
147456.863	CH ₃ OCH ₃	257.141	0.0376	145.57157
147561.719	C ₂ H ₃ CN	38.4910	2.46	232.515
161261.141	C ₂ H ₅ CN	95.144	5.56	213.
161265.734	C ₂ H ₅ CN	108.253	4.72	199.066
b161281.953	CH ₃ OCH ₃	75.305	0.0483	49.41313
161289.996	CH ₃ OCH ₃	333.668	0.0512	162.13361
161303.484	C ₂ H ₅ CN	139.060	3.33	166.301
161304.922	C ₂ H ₅ CN	73.536	3.89	235.93
161367.344	C ₂ H ₅ CN	175.957	2.78	126.974
161379.844	C ₂ H ₅ CN	65.047	2.79	244.939
161397.0470	C ₂ H ₃ CN	97.1140	2.84	434.328
161381.875	C ₂ H ₅ CN	65.047	2.79	244.939
161441.266	C ₂ H ₃ CN	139.0100	2.21	193.130
161445.391	C ₂ H ₃ CN	67.1130	2.94	234.339
161475.172	C ₂ H ₅ CN	52.712	5.04	258.004
161480.219	C ₂ H ₃ CN	164.3800	3.68	178.538
161527.500	C ₂ H ₃ CN	192.6770	1.10	162.238
161581.203	C ₂ H ₅ CN	58.115	4.78	252.312
209422.190	CH ₃ OCH ₃	136.101	0.1111	71.12975
209515.532	CH ₃ OCH ₃	41.221	0.1111	54.9886
209735.828	C ₂ H ₃ CN	86.7860	1.14	315.05
209812.329	CH ₃ OCH ₃	168.885	0.0864	64.85627
224002.109	C ₂ H ₅ CN	166.828	4.21	309.672
224003.438	C ₂ H ₅ CN	152.185	7.58	320.879
224045.750	C ₂ H ₅ CN	200.696	4.21	283.72
224084.281	C ₂ H ₅ CN	219.912	2.95	268.96
224088.203	C ₂ H ₅ CN	127.510	8.01	339.753
224186.344	C ₂ H ₅ CN	262.876	2.63	235.93
224206.609	C ₂ H ₅ CN	117.492	4.01	347.406
224208.078	C ₂ H ₅ CN	117.492	4.01	347.406
224419.812	C ₂ H ₅ CN	109.033	6.01	353.894
224458.859	C ₂ H ₅ CN	109.036	6.01	353.894
237261.970	CH ₃ OCH ₃	214.188	0.1533	66.88355
237396.976	C ₂ H ₃ CN	168.5260	3.14	336.209
237411.906	C ₂ H ₃ CN	149.0560	3.14	343.797
237415.359	C ₂ H ₃ CN	190.9600	2.62	327.453
237456.250	C ₂ H ₃ CN	216.3420	2.32	317.531

237483.891	C ₂ H ₃ CN	132.5690	2.98	700.436
237514.016	C ₂ H ₃ CN	244.6530	1.85	306.440
237548.541	CH ₃ OCH ₃	447.259	0.1533	34.69413
237585.4840	C ₂ H ₃ CN	275.8720	2.04	588.366
237591.3910	C ₂ H ₃ CN	108.5880	2.38	359.528
237620.371	CH ₃ OCH ₃	32.291	0.1533	23.17836
237638.016	C ₂ H ₃ CN	119.0860	3.49	355.471

Table .6: Transitions observed towards G29.96–0.02 during the 1997 observing run.

ν (MHz)	Molecule	E_l (cm ⁻¹)	$\int T_{MB} dv$ (K km s ⁻¹)	$\mu^2 S$ (D ²)
98523.883	C ₂ H ₅ CN	44.251	0.41	113.939
98524.664	C ₂ H ₅ CN	54.287	0.52	96.525
98532.070	C ₂ H ₅ CN	65.860	0.34	76.412
98533.9845	C ₂ H ₅ CN	35.754	0.55	128.685
98564.836	C ₂ H ₅ CN	28.801	0.19	140.761
98566.797	C ₂ H ₅ CN	28.801	0.40	140.761
98701.109	C ₂ H ₅ CN	23.398	0.69	150.140
104177.000	CH ₃ OCH ₃	102.625	0.021	79.56847
104490.168	CH ₃ OCH ₃	585.600	0.027	4.48006
104437.5160	C ₂ H ₃ CN	90.9290	0.353	191.014
111802.17	CH ₃ OCH ₃	42.141	0.024	2.53886
111802.93	CH ₃ OCH ₃	42.142	0.0183	2.53886
b111813.417	CH ₃ OCH ₃	118.013	0.0368	96.5637
b147205.839	CH ₃ OCH ₃	22.082	0.0458	19.52177
147456.863	CH ₃ OCH ₃	257.141	0.040	145.57157
161261.141	C ₂ H ₅ CN	95.144	2.14	213.0
161265.734	C ₂ H ₅ CN	108.253	1.16	199.066
161289.996	CH ₃ OCH ₃	333.668	0.0467	162.13361
161303.484	C ₂ H ₅ CN	139.060	2.14	166.301
161304.922	C ₂ H ₅ CN	73.536	1.43	235.930
161367.344	C ₂ H ₅ CN	175.957	1.79	126.974
161379.844	C ₂ H ₅ CN	65.047	1.34	244.939
161381.875	C ₂ H ₅ CN	65.047	1.34	244.939
161397.047	C ₂ H ₃ CN	97.1140	0.89	217.164
161475.172	C ₂ H ₅ CN	52.712	1.63	258.004

161480.219	C ₂ H ₃ CN	164.3800	0.71	178.538
161581.203	C ₂ H ₅ CN	58.115	1.59	252.312
173083.162	CH ₃ OCH ₃	110.480	0.1542	34.27361
173094.261	CH ₃ OCH ₃	149.025	0.1542	85.5836
173293.064	CH ₃ OCH ₃	34.233	0.1542	46.73276
209735.8280	C ₂ H ₃ CN	86.7860	0.73	315.05
209422.190	CH ₃ OCH ₃	136.101	0.094	71.12975
209515.532	CH ₃ OCH ₃	41.221	0.094	54.9886
209812.329	CH ₃ OCH ₃	168.885	0.0733	64.85627
224002.109	C ₂ H ₅ CN	166.828	1.86	309.672
224003.438	C ₂ H ₅ CN	152.185	1.72	320.879
224017.5310	C ₂ H ₅ CN	183.0000	1.21	594.572
224028.1410	C ₂ H ₅ CN	139.0770	1.08	661.812
224045.750	C ₂ H ₅ CN	200.696	2.19	283.720
224084.281	C ₂ H ₅ CN	219.912	2.09	268.960
224088.2035	C ₂ H ₅ CN	127.510	2.00	339.753
224206.609	C ₂ H ₅ CN	117.492	2.36	347.406
224208.078	C ₂ H ₅ CN	117.492	1.68	347.406
224419.812	C ₂ H ₅ CN	109.033	2.86	353.894
224458.859	C ₂ H ₅ CN	109.036	2.36	353.894
237261.970	CH ₃ OCH ₃	214.188	0.146	66.88355
237396.976	C ₂ H ₃ CN	168.526	1.22	336.209
237548.541	CH ₃ OCH ₃	447.259	0.146	34.69413
237620.371	CH ₃ OCH ₃	32.291	0.146	23.17836

Table .7: Transitions observed towards G29.96-0.02 during the 1996 observing run.

ν (MHz)	Molecule	E_l (cm ⁻¹)	$\int T_{MB} dv$ (K km s ⁻¹)	$\mu^2 S$ (D ²)
b154311.469	CH ₃ OCH ₃	185.5	0.0114	12.859
b154456.5	CH ₃ OCH ₃	62.92	0.063	21.739
215040.8	C ₂ H ₅ CN	229.5	5.22	1199.4
215088.203	C ₂ H ₅ CN	288.76	2.31	533.6
215109.047	C ₂ H ₅ CN	183.46	4.82	651.1
215119.203	C ₂ H ₅ CN	135.84	4.22	369.666
215126.703	C ₂ H ₅ CN	316.4	1.66	502.8
215173.234	C ₂ H ₅ CN	346.23	1.5	469.4

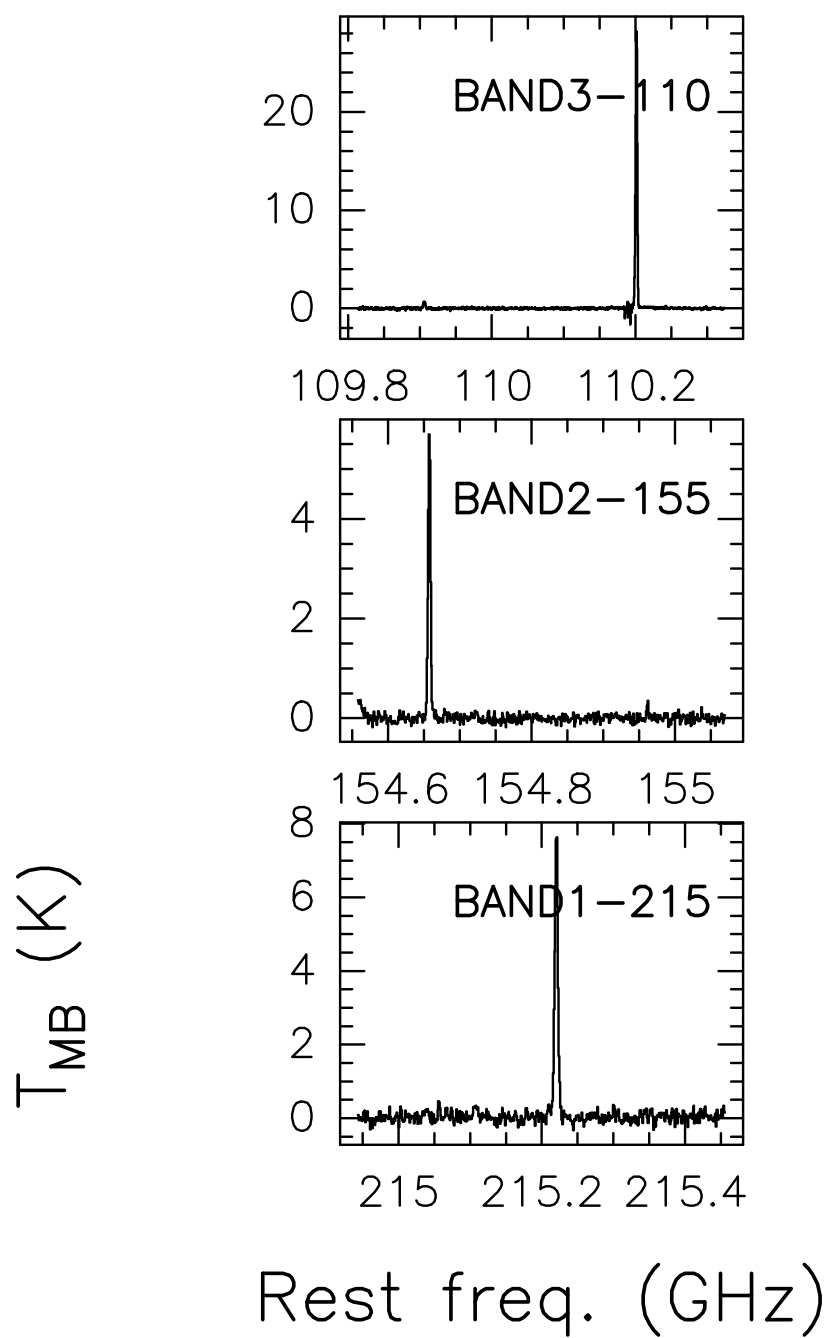
215400.797	C ₂ H ₅ CN	156.87	3.44	340.336
215427.984	C ₂ H ₅ CN	156.88	3.88	340.332

Table .8: Transitions observed towards G31.41+0.31 during the 1997 August observing run.

ν (MHz)	Molecule	E_l (cm ⁻¹)	$\int T_{MB} d\nu$ (K km s ⁻¹)	$\mu^2 S$ (D ²)
98523.883	C ₂ H ₅ CN	44.251	1.60	113.939
98524.664	C ₂ H ₅ CN	54.287	2.00	96.525
98532.070	C ₂ H ₅ CN	65.860	1.80	76.412
98533.9845	C ₂ H ₅ CN	35.754	2.79	128.685
98544.148	C ₂ H ₅ CN	78.967	2.22	53.615
98559.867	C ₂ H ₅ CN	93.604	0.59	28.149
98564.836	C ₂ H ₅ CN	28.801	1.87	140.761
98566.797	C ₂ H ₅ CN	28.801	2.42	140.761
98701.109	C ₂ H ₅ CN	23.398	2.60	150.140
b104177.000	CH ₃ OCH ₃	102.625	0.0843	79.56847
104212.656	C ₂ H ₃ CN	23.411	1.18	155.205
104419.312	C ₂ H ₃ CN	71.464	1.48	112.653
104432.7970	C ₂ H ₃ CN	30.9450	1.13	148.58
104453.930	C ₂ H ₃ CN	30.9460	1.62	148.580
104490.168	CH ₃ OCH ₃	585.600	0.0424	4.48006
b 111574.6250	C ₂ H ₅ CN	73.7330	0.38	10.807
b111742.636	CH ₃ OCH ₃	130.299	0.1514	103.90668
b111783.241	CH ₃ OCH ₃	17.550	0.1647	27.2197
b111801.945	CH ₃ OCH ₃	42.142	0.029	4.43093
b111813.417	CH ₃ OCH ₃	118.013	0.1694	96.5637
b147205.839	CH ₃ OCH ₃	22.082	0.3239	19.52177
b147456.863	CH ₃ OCH ₃	257.141	0.0816	145.57157
147561.719	C ₂ H ₃ CN	38.4910	2.66	232.515
161261.141	C ₂ H ₅ CN	95.144	7.89	213.
161265.734	C ₂ H ₅ CN	108.253	6.91	199.066
b161281.953	CH ₃ OCH ₃	75.305	0.1839	49.41313
161289.996	CH ₃ OCH ₃	333.668	0.0667	162.13361
161303.484	C ₂ H ₅ CN	139.060	5.67	66.301
161304.922	C ₂ H ₅ CN	73.536	3.70	235.93
161367.344	C ₂ H ₅ CN	175.957	2.47	126.974

161379.844	C ₂ H ₅ CN	65.047	3.86	244.939
161381.875	C ₂ H ₅ CN	65.047	4.12	244.939
161397.047	C ₂ H ₃ CN	97.114	3.62	217.164
161447.8750	C ₂ H ₃ CN	67.1130	5.4	468.678
161475.172	C ₂ H ₅ CN	52.712	8.24	258.004
161502.266	C ₂ H ₃ CN	56.605	2.16	240.337
161581.203	C ₂ H ₅ CN	58.115	5.92	252.312
172998.766	C ₂ H ₅ CN	55.578	9.50	293.998
173092.859	C ₂ H ₃ CN	54.7720	11.2	259.424
173083.162	CH ₃ OCH ₃	110.480	0.3097	34.27361
173094.261	CH ₃ OCH ₃	149.025	0.1542	85.5836
b173293.064	CH ₃ OCH ₃	34.233	0.4182	46.73276
b209515.532	CH ₃ OCH ₃	41.221	0.479	54.9886
209812.329	CH ₃ OCH ₃	168.885	0.1334	64.85627
224002.109	C ₂ H ₅ CN	166.828	5.36	309.672
224003.438	C ₂ H ₅ CN	152.185	6.13	320.879
224045.75	C ₂ H ₅ CN	200.696	6.72	283.720
224084.281	C ₂ H ₅ CN	219.912	4.60	268.960
224088.2035	C ₂ H ₅ CN	127.510	6.89	339.753
224131.516	C ₂ H ₅ CN	240.640	3.82	253.034
224186.344	C ₂ H ₅ CN	262.876	3.73	235.930
224206.609	C ₂ H ₅ CN	117.492	5.22	347.406
224208.078	C ₂ H ₅ CN	117.492	5.22	347.406
224248.016	C ₂ H ₅ CN	286.614	1.91	217.645
224419.812	C ₂ H ₅ CN	109.033	7.66	353.894
224458.859	C ₂ H ₅ CN	109.036	7.63	353.894
237396.9765	C ₂ H ₃ CN	168.526	2.50	336.209
237405.1880	C ₂ H ₅ CN	101.8870	8.49	380.894
b237476.0470	C ₂ H ₅ CN	91.4820	3.77	19.864
237456.250	C ₂ H ₃ CN	216.3420	2.10	317.531
237485.016	C ₂ H ₃ CN	132.5700	3.12	350.218
237548.541	CH ₃ OCH ₃	447.259	0.1445	34.69413
237591.3910	C ₂ H ₃ CN	108.5880	2.17	359.528
b237620.371	CH ₃ OCH ₃	32.291	0.452	23.17836
237638.0160	C ₂ H ₃ CN	119.0860	2.17	355.471
237668.7660	C ₂ H ₃ CN	309.9800	2.03	561.516

g10.62

**Fig. .4.** Same as Fig. .2 for G10.62.

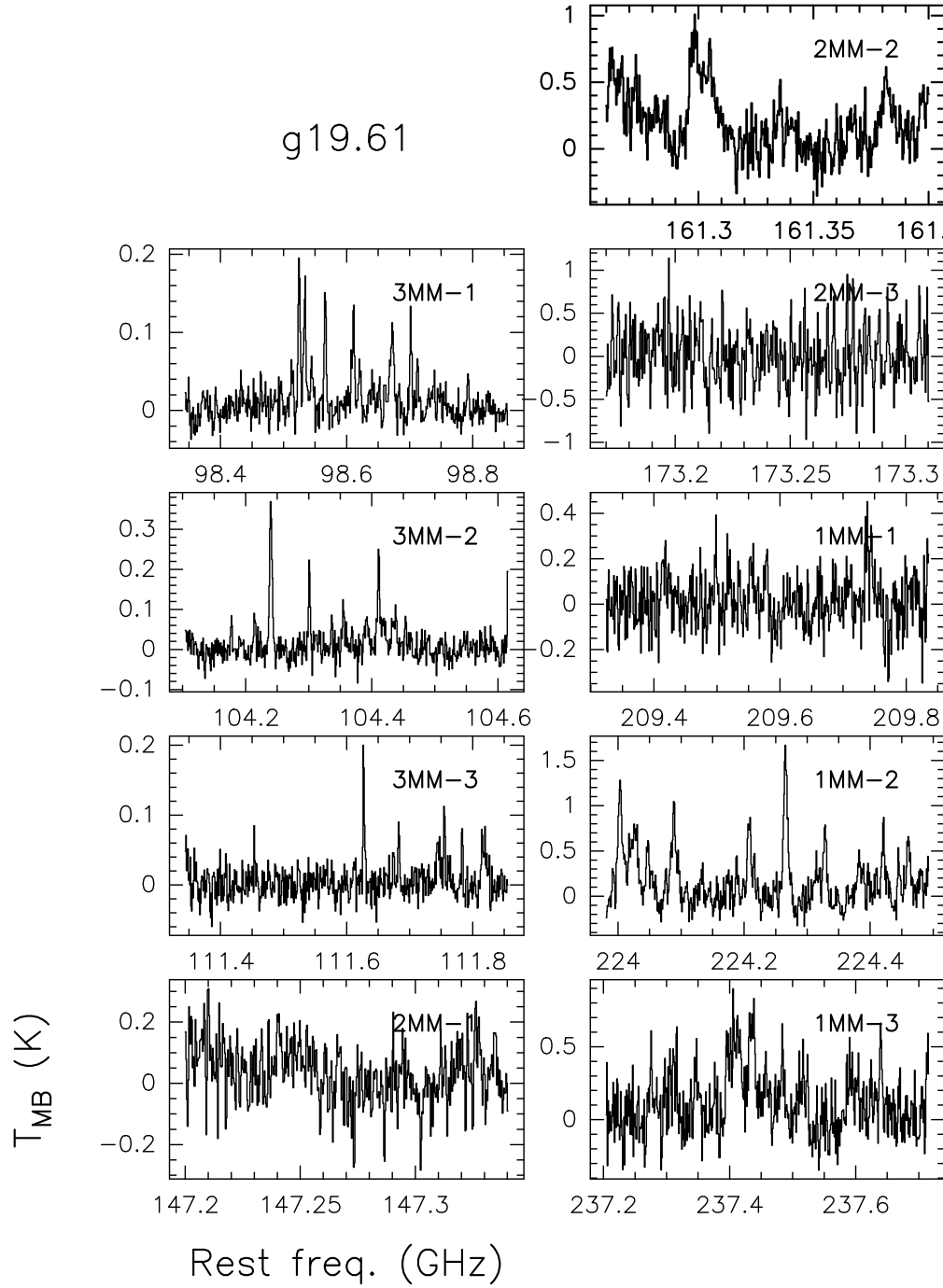


Fig. 5. Same as Fig. 1 for G19.61.

Table 9: Transitions observed towards G31.41+0.31 during the 1996 July observing run.

ν (MHz)	Molecule	E_l (cm ⁻¹)	$\int T_{MB} dv$ (K km s ⁻¹)	$\mu^2 S$ (D ²)
b140226.172	CH ₃ OCH ₃	159.81	0.0686	9.896
a140429.484	C ₂ H ₅ CN	54.24	2.2	202.872

b154027.062	C ₂ H ₅ CN	10.02	2.64	2.344
b154311.469	CH ₃ OCH ₃	185.5	0.035	12.855
b154456.5	CH ₃ OCH ₃	62.92	0.2081	21.739
154724.531	C ₂ H ₅ CN	65.42	5.75	215.731
215040.8	C ₂ H ₅ CN	229.5	15.9	1199.4
215088.203	C ₂ H ₅ CN	288.76	8.46	533.6
215109.047	C ₂ H ₅ CN	183.46	12.49	651.1
215119.203	C ₂ H ₅ CN	135.84	12.63	369.666
215126.703	C ₂ H ₅ CN	316.4	6.56	502.8
215173.234	C ₂ H ₅ CN	346.23	5.91	469.4
215400.797	C ₂ H ₅ CN	156.87	11.84	340.336
215427.984	C ₂ H ₅ CN	156.88	12.85	340.332
227897.625	C ₂ H ₅ CN	242.47	6.59	594.744
227906.719	C ₂ H ₅ CN	214.46	6.89	609.457
227918.656	C ₂ H ₅ CN	274.75	3.33	577.798
227960.234	C ₂ H ₅ CN	311.27	3.03	558.56
227967.594	C ₂ H ₅ CN	190.74	6.87	621.8
228017.375	C ₂ H ₅ CN	352.	3.44	537.313
228087.297	C ₂ H ₅ CN	396.91	0.91	513.431
228090.531	C ₂ H ₅ CN	156.23	5.45	319.903
228104.609	C ₂ H ₅ CN	171.34	5.45	315.959
228160.297	C ₂ H ₅ CN	171.35	7.02	631.917

Table .10: Transitions observed towards G34.26+0.15 during the 1997 observing run.

ν (MHz)	Molecule	E_l (cm ⁻¹)	$\int T_{MB} d\nu$ (K km s ⁻¹)	$\mu^2 S$ (D ²)
98523.883	C ₂ H ₅ CN	44.251	1.23	113.939
98524.664	C ₂ H ₅ CN	54.287	0.96	96.525
98532.070	C ₂ H ₅ CN	65.860	1.16	76.412
98533.9845	C ₂ H ₅ CN	35.754	1.64	128.685
98544.148	C ₂ H ₅ CN	78.967	0.68	53.615
98559.867	C ₂ H ₅ CN	93.604	0.24	28.149
98564.836	C ₂ H ₅ CN	28.801	1.10	140.761
98566.797	C ₂ H ₅ CN	28.801	1.35	140.761
98701.109	C ₂ H ₅ CN	23.398	1.37	150.140
b104177.000	CH ₃ OCH ₃	102.625	0.1033	79.56847

104419.312	C ₂ H ₃ CN	71.4640	0.57	112.653
104432.797	C ₂ H ₃ CN	30.9450	0.57	148.58
104437.516	C ₂ H ₃ CN	90.9290	0.71	95.507
104453.930	C ₂ H ₃ CN	30.9460	0.89	148.58
104461.5160	C ₂ H ₃ CN	113.3510	0.425	151.236
b111783.241	CH ₃ OCH ₃	17.550	0.1639	27.2197
111802.93	CH ₃ OCH ₃	42.142	0.0192	2.53886
b111813.417	CH ₃ OCH ₃	118.013	0.1493	96.5637
b147205.839	CH ₃ OCH ₃	22.082	0.2814	19.52177
b147456.863	CH ₃ OCH ₃	257.141	0.0763	145.57157
161261.141	C ₂ H ₅ CN	95.144	9.19	213.
161265.734	C ₂ H ₅ CN	108.253	6.32	199.066
b161285.603	CH ₃ OCH ₃	75.305	0.279	12.35331
161289.996	CH ₃ OCH ₃	333.668	0.0566	162.13361
161303.484	C ₂ H ₅ CN	139.060	6.89	166.301
161304.922	C ₂ H ₅ CN	73.536	6.89	235.930
161367.344	C ₂ H ₅ CN	175.957	2.87	126.974
161379.844	C ₂ H ₅ CN	65.047	6.24	244.939
161381.875	C ₂ H ₅ CN	65.047	4.05	244.939
161397.047	C ₂ H ₃ CN	97.1140	2.31	217.164
161445.391	C ₂ H ₃ CN	67.1130	2.21	234.339
161450.359	C ₂ H ₃ CN	67.1130	2.21	234.339
161475.172	C ₂ H ₅ CN	52.712	7.47	258.004
161581.203	C ₂ H ₅ CN	58.115	5.75	252.312
172998.766	C ₂ H ₅ CN	55.578	5.92	293.998
173092.859	C ₂ H ₃ CN	54.7720	4.69	259.424
b173293.064	CH ₃ OCH ₃	34.233	0.3016	46.73276
b209515.532	CH ₃ OCH ₃	41.221	0.7994	54.9886
b209812.329	CH ₃ OCH ₃	168.885	0.1865	64.85627
224002.109	C ₂ H ₅ CN	166.828	9.23	309.672
224003.438	C ₂ H ₅ CN	152.185	3.69	320.879
224045.75	C ₂ H ₅ CN	200.696	3.26	283.720
224084.281	C ₂ H ₅ CN	219.912	3.88	268.960
224088.2035	C ₂ H ₅ CN	127.510	6.79	339.753
224186.344	C ₂ H ₅ CN	262.876	2.43	235.930
224206.609	C ₂ H ₅ CN	117.492	4.95	347.406
224208.078	C ₂ H ₅ CN	117.492	4.95	347.406
b224310.9220	C ₂ H ₃ CN	84.2220	5.83	2.17

224315.9380	C ₂ H ₅ CN	311.8460	2.62	396.362
224419.812	C ₂ H ₅ CN	109.033	5.32	353.894
224458.859	C ₂ H ₅ CN	109.036	5.64	353.894
237396.969	C ₂ H ₃ CN	168.5260	1.40	336.209
237405.1880	C ₂ H ₅ CN	101.8870	9.42	380.894
237411.906	C ₂ H ₃ CN	149.0560	1.67	343.797
237485.016	C ₂ H ₃ CN	132.5700	1.50	350.218
237548.541	CH ₃ OCH ₃	447.259	0.152	34.69413
b237620.371	CH ₃ OCH ₃	32.291	0.443	23.17836
237638.016	C ₂ H ₃ CN	119.0860	1.76	355.471

Table .11. Transitions observed towards G34.26+0.15 during the 1996 observing run.

ν (MHz)	Molecule	E_l (cm ⁻¹)	$\int T_{MB} dv$ (K km/s)	$\mu^2 S$ (D ²)
215040.8	C ₂ H ₅ CN	229.5	15.83	1199.4
215088.203	C ₂ H ₅ CN	288.76	7.	533.6
215109.047	C ₂ H ₅ CN	183.46	10.73	651.1
215119.203	C ₂ H ₅ CN	135.84	11.35	369.666
215126.703	C ₂ H ₅ CN	316.4	4.87	502.8
215173.234	C ₂ H ₅ CN	346.23	4.37	469.4
215400.797	C ₂ H ₅ CN	156.87	9.2	340.336
215427.984	C ₂ H ₅ CN	156.88	11.88	340.332

Appendix C: Boltzmann plots

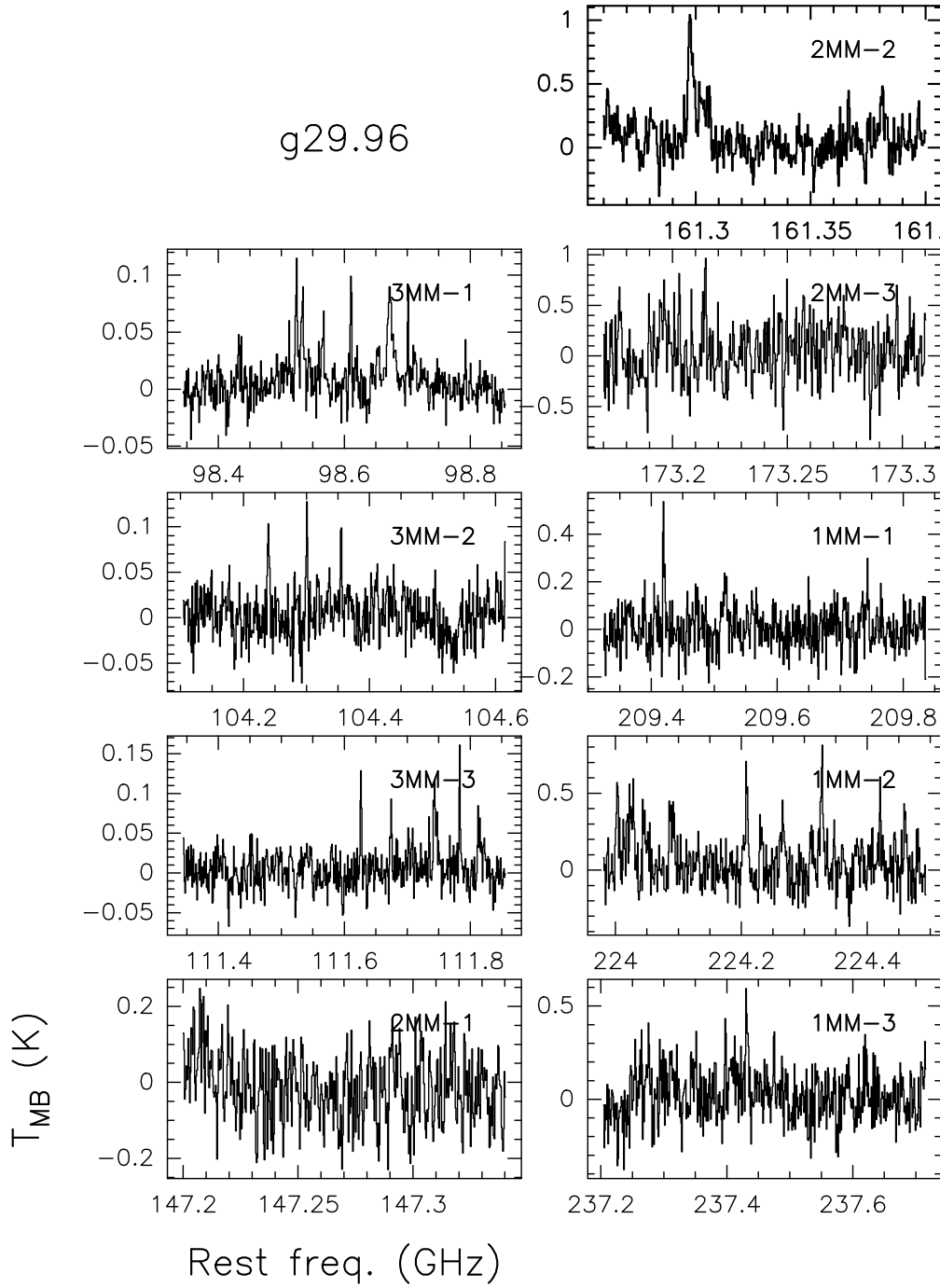


Fig. .6. Same as Fig. .1 for G29.96.

References

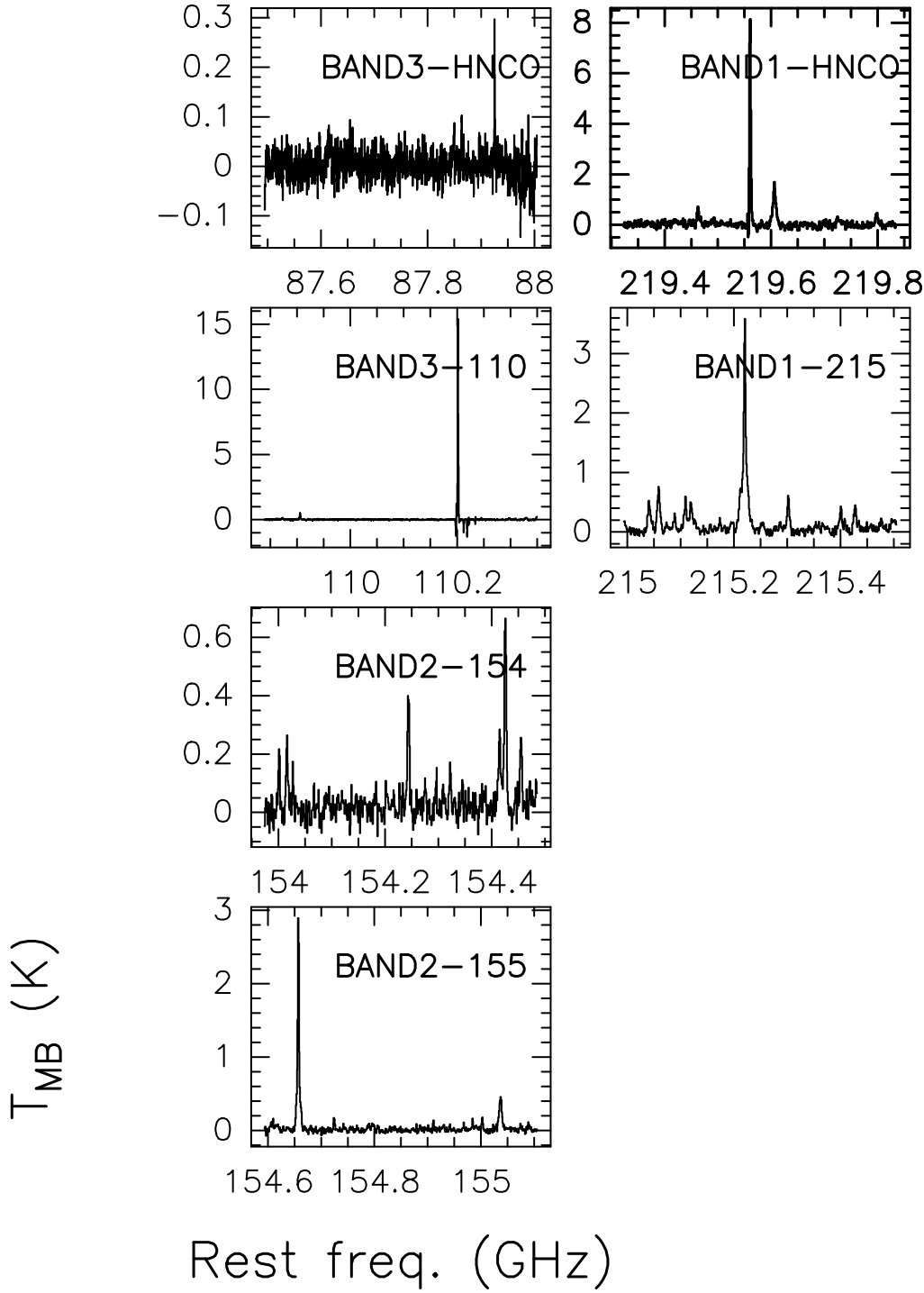
- Acord, J.M., Churchwell, E., Wood, D.O.S. 1998, *ApJ* 495, L107
- Akeson R.L. & Carlstrom J.E. 1996, *ApJ*, 470, 528
- Allen, M., & Robinson, G. W. 1977, *ApJ*, 212, 396
- Anderson T., Herbst E., de Lucia F. C. 1987, *ApJS*, 64, 703
- Anderson T., Crownover R. L., Herbst E., De Lucia F. C. 1988a *ApJS*, 67,135
- Anderson T., Herbst E., de Lucia F. C. 1988b, *ApJS*, 68, 821

- Anderson T., de Lucia F. C., Herbst E. 1990a, *ApJS*, 72, 797
- Anderson T., Herbst E., de Lucia F. C. 1990b, *ApJS*, 74, 647
- Anderson T., Herbst E., de Lucia F. C. 1992, *ApJS*, 82, 405
- Avalos, M., Lizano, S., Rodríguez, L.F., Franco-Hernández, R., Moran, J.M. 2006, *ApJ*, 641, 406
- Beltrán, M.T., Cesaroni, R., Neri, R. et al., 2005, *A&A*, 435, 901
- Bettens F. L., Sastry K. V. L. N., Herbst E., Albert S., Oesterling Lee C., de Lucia F. C. 1999, *ApJ* 510, 789
- Beuther, H., Churchwell, E. B., McKee, C.F., Tan, J.C. 2007, *Protostars and Planets V*, ed. B. Reipurth, D. Jewitt, and K. Keil, University of Arizona Press, Tucson, p.165
- Beuther, H., Zhang, Q., Greenhill, L. J., et al. 2005, *ApJ*, 632, 355
- Bisschop, S.E., Jorgensen, J.K., van Dishoeck, E.F., de Wachter, E.B.M. 2007, *A&A* in press, astro-ph/0702066
- Blake G. A., Sutton E. C., Masson C. R., Phillips T. G. 1987, *ApJ*, 315, 621
- Carral P. & Welch W. J. 1992, *ApJ*, 385, 244
- Caselli P., Hasegawa T. I., Herbst E. 1993, *ApJ*, 408, 548
- Caselli, P. 2005, in “Cores to Clusters: Star Formation with Next Generation Telescopes. Ed. by M.S. Nanda Kumar, M. Tafalla and P. Caselli. Published by Springer, New York, NY USA, p. 47
- Cesaroni R., Walmsley C. M., Kömpe C., Churchwell E. 1991, *A&A*, 252, 278
- Cesaroni R., Hofner P., Walmsley C. M., Churchwell E. 1998, *A&A*, 331, 709
- Cesaroni, R. 2005, Proceedings of the IAUS227 “Massive Star Birth: A Crossroads of Astrophysics”
- Cesaroni, R., Galli, D., Lodato, G., Walmsley, C.M. & Zhang, Q. 2007, *Protostars and Planets V*, ed. by B. Reipurth, D. Jewitt, and K. Keil, University of Arizona Press, Tucson, p. 197
- Charnley S. B., Tielens A. G. G. M., Millar T. J. 1992, *ApJ*, 399, L71
- Charnley S. B. 1995, *Ap&SS* 224, 251
- Churchwell E., Walmsley C. M., Cesaroni R. 1990, *A&AS*, 83, 119
- Comito, C., Schilke, P., Phillips, T.G., et al. 2005, *ApJS*, 156, 127
- Fish, V.L., Reid, M.J., Wilner, D.J., Churchwell, E. 2003, *ApJ*, 587, 701
- Fontani, F., Cesaroni, R., Caselli, P. et al. 2002, *A&A*, 389, 603
- Garay G. & Rodríguez L.F. 1990, *ApJ*, 362, 191
- Garay G., Moran J.M., Rodríguez L.F., Reid M.J. 1998, *ApJ*, 492, 635
- Garay G., Lizano S. 1999, *PASP*, 111, 1049
- Garrod, R.T. & Herbst, E. 2006, *A&A*, 457, 927
- Genzel R., Stutzki J. 1989, *Annu. Rev. Astron. Astrophys.*, 27, 41
- Genzel R., “The galactic interstellar medium” Saas-Fee Advanced Course 21, 1991 ed. Springer-Verlag Berlin Heidelberg 1992
- Gibb, E., Nummelin, A., Irvine, W.M., Whittet, D.C.B., Bergman, P. 2000, *ApJ*, 545, 309

- Gibb, A.G., Wyrowski, F., Mundy, L.G. 2004, *ApJ*, 616, 301
- Goldsmith P. F. & Langer W. D. 1999, *ApJ*, 519, 173
- Groner P., Albert S., Herbst E., de Lucia F. C. 1998, *ApJ*, 500, 1059
- Hatchell J., Thompson M. A., Millar T. J., Macdonald G. H. 1998, *A&AS*, 133, 29
- Herbst E. 1999 "HCOOCH₃ transitions", private communication
- Hofner P., Wyrowski F., Walmsley C. M., Churchwell E. 2000, *ApJ*, 536, 393
- Ho P. T. P. & Haschick A. D. 1986, *ApJ*, 304, 501
- Keto E. R., Ho P. T. P., Haschick A. D., Aubrey D. 1987, *ApJ*, 318, 712
- Keto E. R., Ho P. T. P., Haschick A. D. 1988, *ApJ*, 324, 920
- Klisch E., Klaus Th., Belov S. P., Dolgner A., Schieder R., Winnewisser G., Herbst E. 1996, *ApJ*, 473, 1118
- Kolpak, M.A., Jackson, J.M., Bania, T.M., Clemens, D.P., Dickey, J.M. 2003, *ApJ*, 582, 756
- Kuchar, T.A. & Bania, T.M. 1994, *ApJ*, 436, 117
- Kurtz S., Cesaroni R., Churchwell E., Hofner P., Walmsley C. M. 2000, "Protostars and Planets IV", eds Mannings, V., Boss, A. P., Russel, S. S. (Tucson: Univ. Arizona Press), p. 299
- Macdonald, G.H., Habing, R.J., Millar, T.J. 1995, *Ap&SS*, 224, 177
- Mehring, D.M., Pearson, J.C., Keene, J., Phillips, T.G. 2004, *ApJ*, 608, 306
- Mookerjea, B., Casper, E., Mundy, L.G., Looney, L.W. 2007, *ApJ*, in press, astro-ph/0701827
- Nomura, H., & Millar, T.J. 2004, *A&A*, 414, 409
- Nummelin, A., Bergman, P., Hjalmarson, A. et al. 1998, *ApJS*, 117, 427
- Nummelin, A. & Bergman, P. 1999, *A&A*, 341, 59L
- Nummelin, A., Bergman, P., Hjalmarson, A. et al. 2000, *ApJS*, 128, 213
- Olmi L., Cesaroni R., Neri R., Walmsley C.M. 1996, *A&A*, 315, 565
- Olmi, L., Cesaroni, R., Hofner, P. et al. 2003, *A&A*, 407, 225
- Pan J., Albert S., Sastry K. V. L. N., Herbst E., de Lucia F. C. 1998, *ApJ* 499, 517
- Pearson J. C., Anderson T., Herbst E., de Lucia F. C., Helminger P. 1991, *ApJ*, 379, L41
- Pearson J. C., Sastry K. V. L. N., Herbst E., de Lucia F. C. 1994, *ApJS*, 93, 589
- Pearson J. C., Sastry K. V. L. N., Herbst E., de Lucia F. C. 1997, *ApJ*, 480, 420
- Pearson J. C. 2002, "C₂H₅CN transitions", personal communication
- Plummer G. M., Herbst E., de Lucia F. C., Blake G. A. 1986, *ApJS*, 60, 949
- Plummer G. M., Herbst E., de Lucia F. C. 1987, *ApJ*, 318, 873
- Pickett H. M., Poynter R. L., Cohen E. A., Delitsky M. L., Pearson J. C., Müller H. S. P. "Submillimeter, millimeter and microwave line catalogue", JPL Publication 80-23, revision 4, Pasadena CA, 1996
- Poynter R. L. & Pickett, H. M. 1985, *Applied Optics*, 24, 2235
- Remijan, A., Shiao, Y.S., Friedel, D.N., Meier, D.S., Snyder, L.E. 2004, *ApJ*, 617, 384
- Rodgers S. D. & Charnley S. B. 2001, *ApJ*, 546, 324
- Schilke P., Groesbeck T. D., Blake G. A., Phillips T. G. 1997, *ApJS*, 108, 301
- Sewilo, M., Churchwell, E., Kurtz, S., Goss, W.M., Hofner, P. 2004, *ApJ*, 605, 285

- Sollins, P.K., Zhang, Q., Keto, E., Ho, P.T.P. 2005, *ApJ*, 624, L49
- Sutton, E.C., Peng, R., Danchi, W.C. et al. 1995, *ApJS*, 97, 455
- Tan, J.C., McKee, C.F. 2002, in *ASP Conf. Ser. 267, The Earliest Stages of Massive Star Birth*, ed. P.A. Crowther (San Francisco: ASP), 267
- Turner B.E. 1991, *ApJS*, 76, 617
- Xu, Y., Reid, M. J., Zheng, X. W., Menten, K. M. 2006, *Science*, 311, 54
- Walmsley C. M., Schilke, P. 1992, *Proceedings of the 50th Symposium of the International Astronomical Union*
- Wright, M., Sandell, G., Wilner, D.J., Plambeck, R.L. 1992, *ApJ*, 393, 225
- Wright M. C. H., Plambeck R. L., Wilner D. J. 1996, *ApJ*, 469, 216
- Wood D. O. S., Churchwell E. 1989, *ApJS*, 69, 831
- Wood D. O. S., Churchwell E. 1990, *ApJS*, 354, 247
- Wyrowski F., Schilke P., Walmsley C.M., Menten, K.M. 1999, *A&A*, 514, L43
- Yamada K. M. T., Creswell R. A. 1986, *J.Mol.Spectr.* 116, 384
- Yorke, H.W. 2004, *Proceedings of the IAU symposium 221*, 141

g29.96

**Fig..7.** Same as Fig. .2 for G29.96.

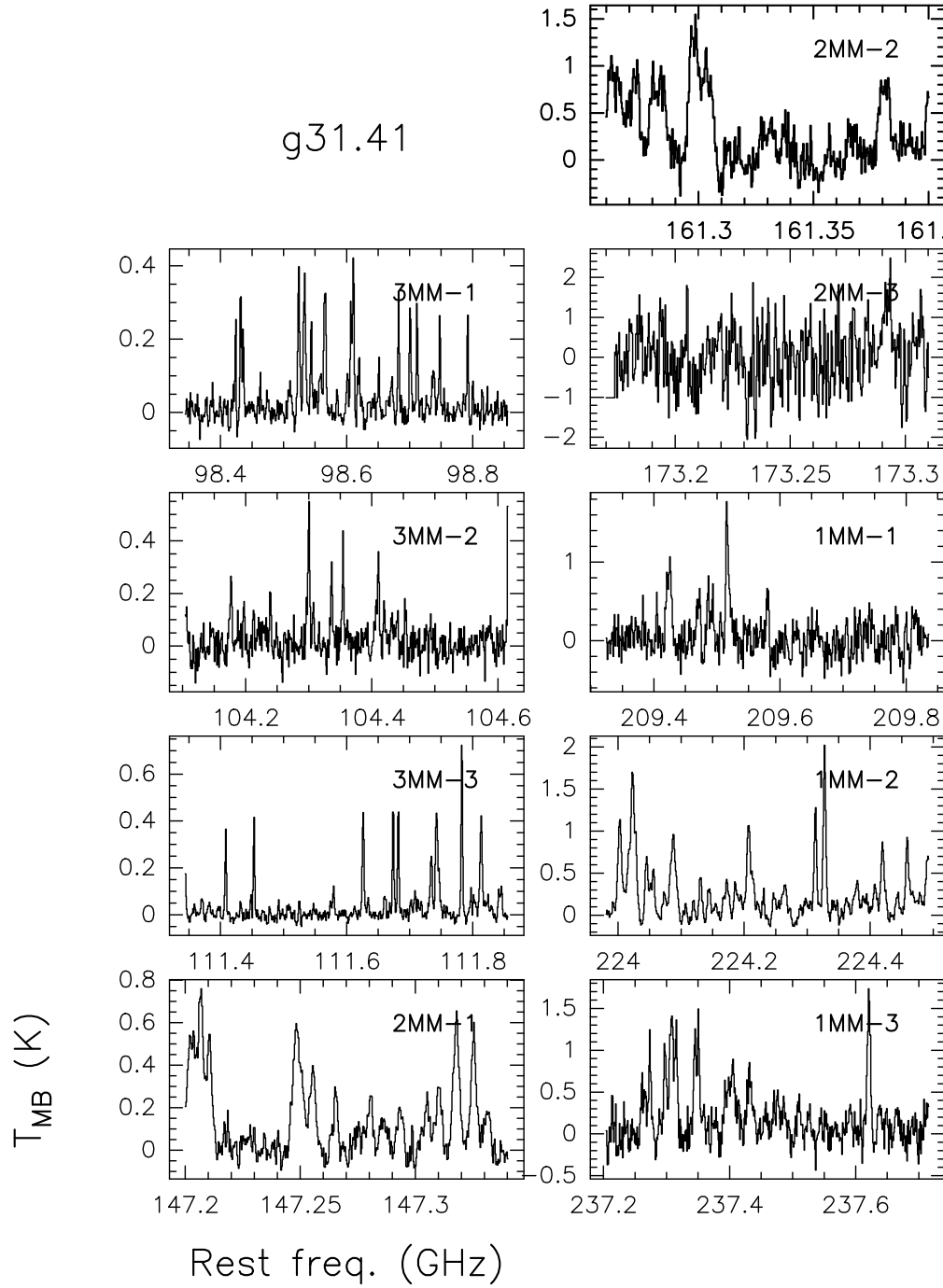
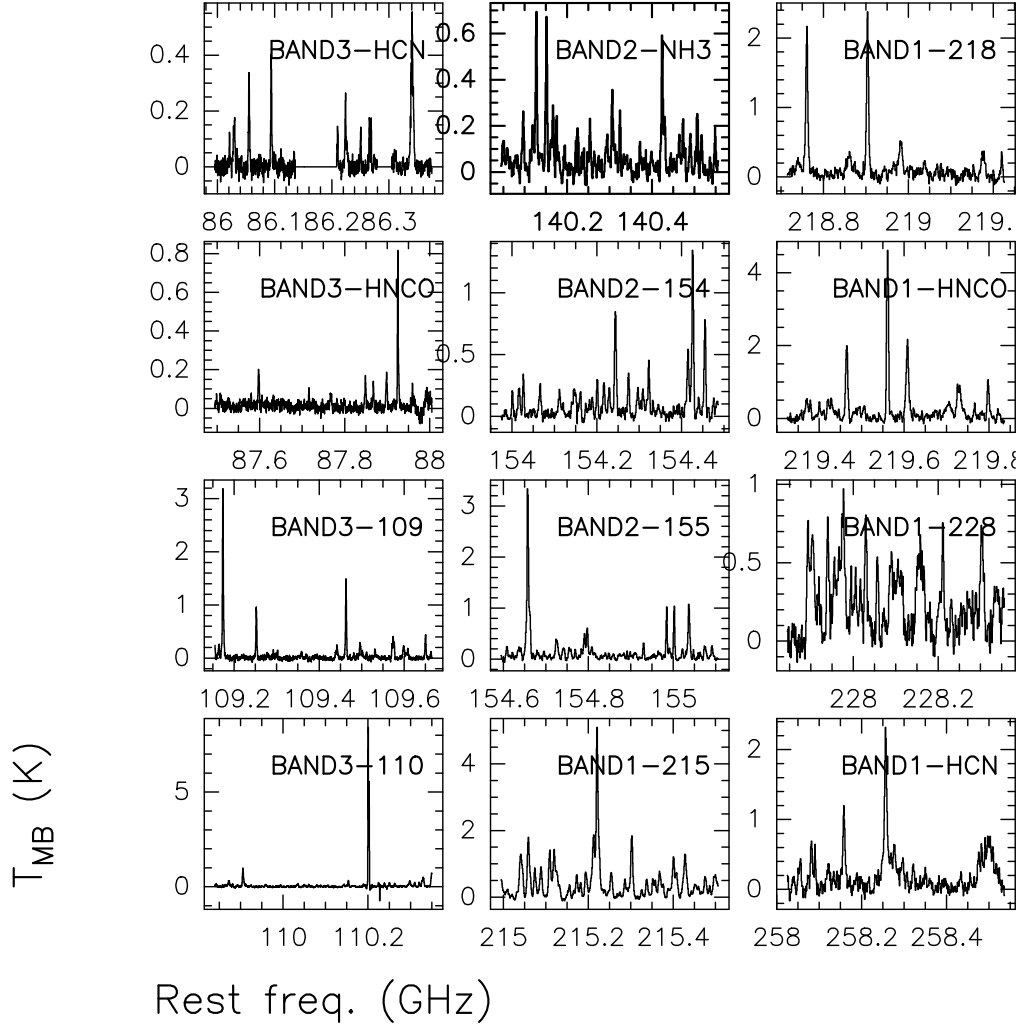


Fig..8. Same as Fig. .1 for G31.41.

g31.41

**Fig. 9.** Same as Fig. 2 for G31.41.

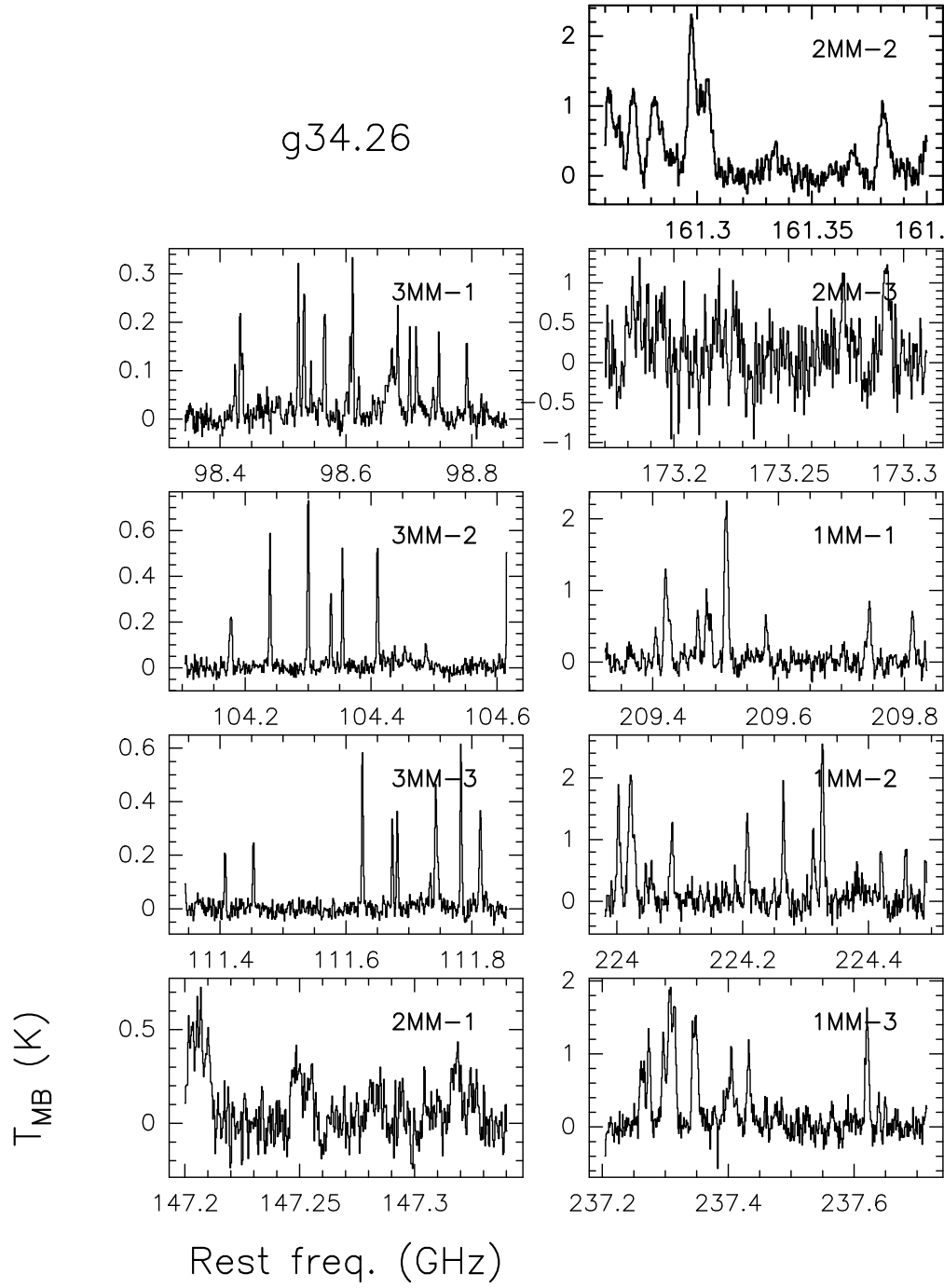
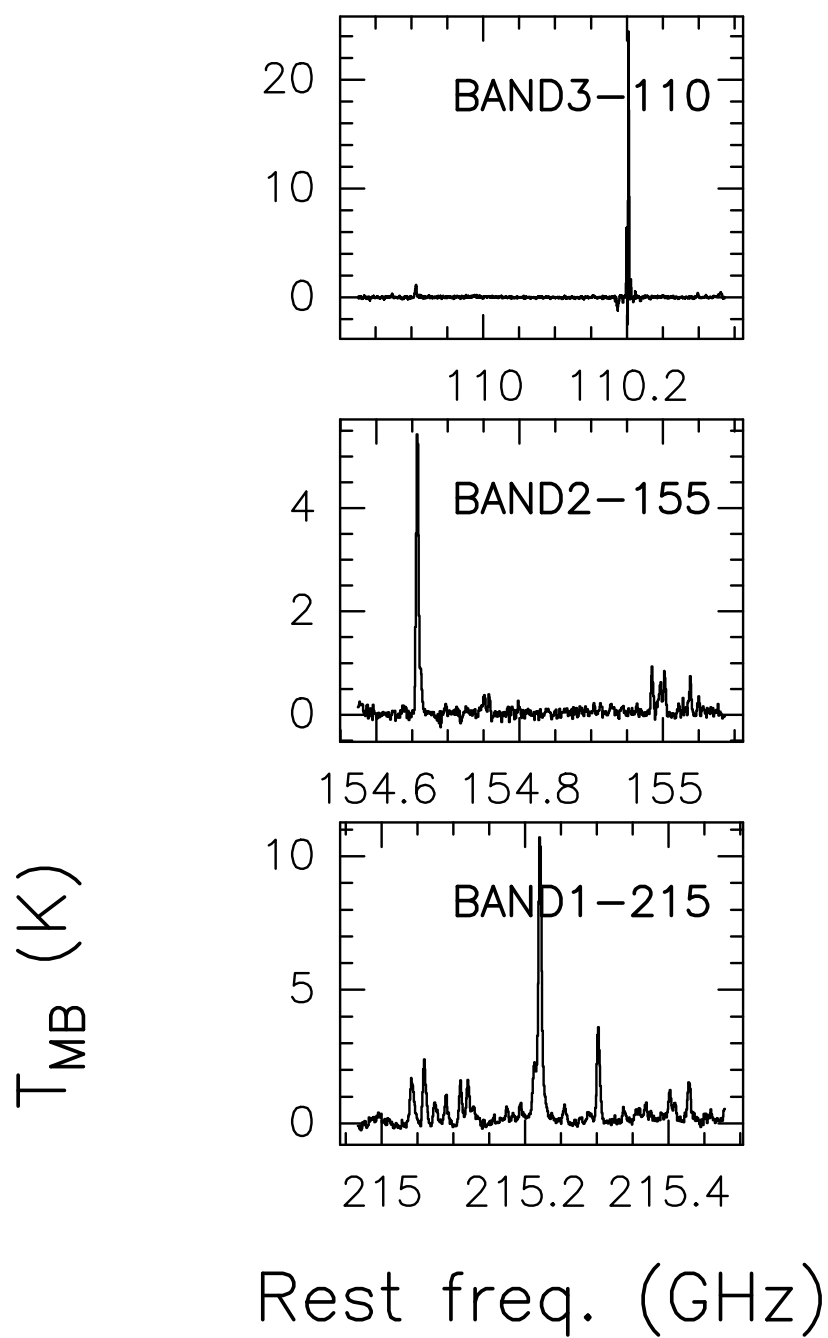


Fig. 10. Same as Fig. 1 for G34.26.

g34.26

**Fig. .11.** Same as Fig. .2 for G34.26.

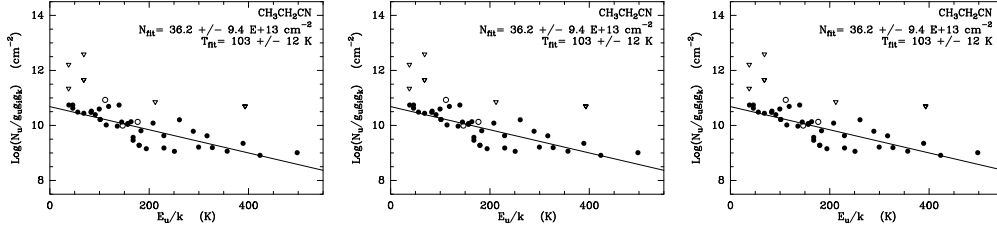


Fig. .1. Boltzmann plots for G10.47. T_{fit} and N_{fit} are the “best-fit” values for the rotational temperature and the total column densities (see Tab. 4). Filled circles indicate “strong” transitions; open circles correspond to “weak” transitions. Open triangles indicate upper limits for undetected lines, estimated from the 3σ level in the spectrum. The error on the quantity on the y-axis is about 20% , and it is due to calibration uncertainties.

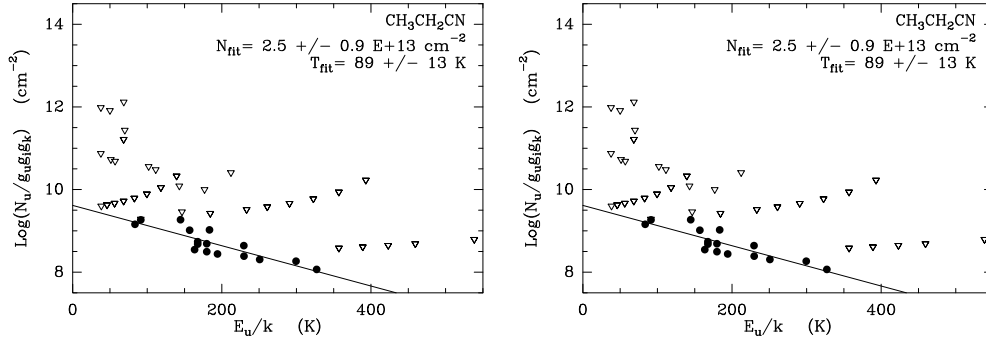


Fig. .2. Same as Fig. .1, but for G10.62.

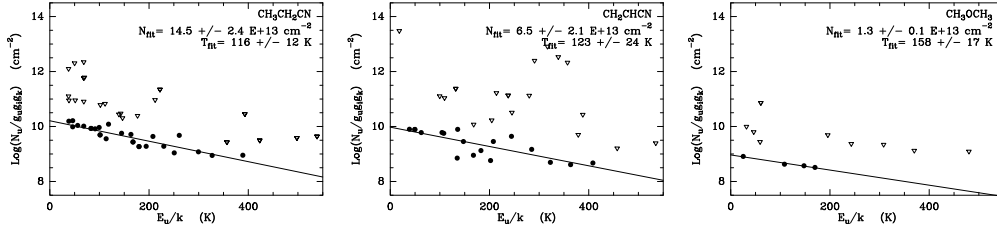


Fig. .3. Same as Fig. .1, but for G19.61.

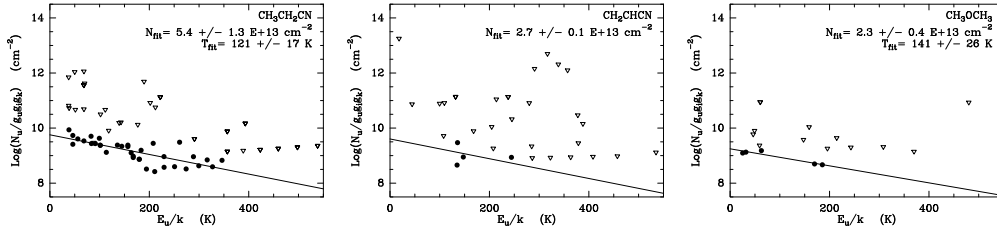


Fig. .4. Same as Fig. .1, but for G29.96.

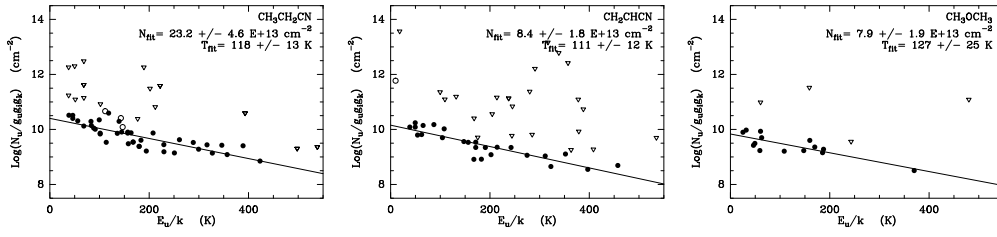


Fig. 5. Same as Fig. .1, but for G31.41.

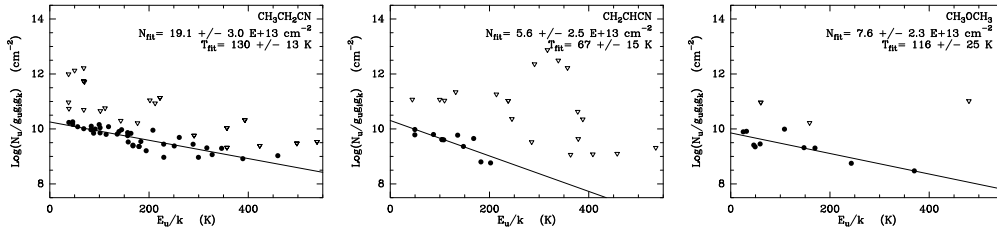


Fig. 6. Same as Fig. .1, but for G34.26.

